

STATUS OF THESIS

Title of thesis Numerical Study of Different Orifices Shapes Effect on the Hydrodynamics of Bubbling Fluidized Bed

I MUHAMAD HILMEE BIN IBRAHIM

hereby allow my thesis to be placed at the Information Resources Center (IRC) of Universiti Teknologi PETRONAS (UTP) with the following condition:

1. The thesis becomes the property of UTP
2. The IRC of UTP may make copies of the thesis for academic purpose only.
3. This thesis is classified as

Confidential

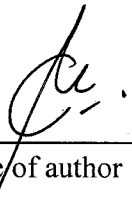
Non-Confidential

If this thesis is confidential, please state the reason:

The contents of the thesis will remain confidential for _____ years.

Remarks on disclosure:

Endorsed By,



Signature of author

Permanent address:
A-1-8 Desa Saujana Condominium,
Taman Sungai Besi Indah, Jln Sgbesi Indah 3,
43300 Seri Kembangan Selangor

Date :



Signature of Supervisor **Dr. S. Chandra Mohan**
Associate Professor
FASD

Name of Supervisor : **Universiti Teknologi PETRONAS**
Assoc. Prof Dr. Chandra Mohan

Date :

UNIVERSITI TEKNOLOGI PETRONAS

NUMERICAL STUDY OF DIFFERENT ORRIFICES SHAPES EFFECT ON THE
HYDRODYNAMICS OF BUBBLING FLUIDIZED BED

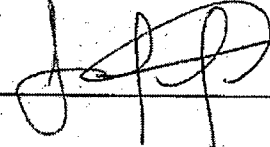
By

MUHAMAD HILMEE BIN IBRAHIM

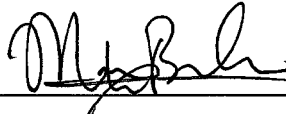
The undersigned certified that they have read, and recommend to the Postgraduate Studies Programme for acceptance this thesis for the fulfilment of the requirements for the degree stated.

Signature : 
: ~~Dr. S. Chandra Mohan~~
Associate Professor
FASD

Main Supervisor : DR. CHANDRA MOHAN

Signature : 
: Dr. Saravanan Karuppanan
Mechanical Engineering Department
Universiti Teknologi PETRONAS
Bandar Seri Iskandar, 31750 Tronoh
Perak Darul Ridzuan, Malaysia.

Co-Supervisor : DR. SARAVANAN KARUPPANAN

Signature : 
:

Head of Department : DR. IR MOHD BASRI
Ir. Dr. Masri Baharom
Head of Department/Associate Professor
Department of Mechanical Engineering
Universiti Teknologi PETRONAS
Bandar Seri Iskandar, 31750 Tronoh,
Perak Darul Ridzuan, Malaysia

Date : 17/12/2013

NUMERICAL STUDY OF DIFFERENT ORRIFICES SHAPES EFFECT ON THE
HYDRODYNAMICS OF BUBBLING FLUIDIZED BED

by

MUHAMAD HILMEE BIN IBRAHIM

A thesis

Submitted to the Post Graduate Studies Programme

As a Requirement of Degree of

MASTER OF SCIENCE

IN MECHANICAL ENGINEERING

UNIVERSITI TEKNOLOGI PETRONAS

BANDAR SERI ISKANDAR

PERAK

DECEMBER 2013

DECLARATION OF THESIS

Title of thesis

Numerical Study of Different Orifices Shapes Effect on the Hydrodynamics of Bubbling Fluidized Bed

I MUHAMAD HILMEE BIN IBRAHIM

hereby declare that the thesis is based on my original work except for quotations and citations which have been duly acknowledged. I also declare that it has not been previously or concurrently submitted for any other degree at UTP or other institutions.

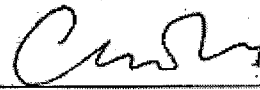
Witnessed by



Signature of author

Permanent address:
A-1-8 Desa Saujana Condominium,
Taman Sungai Besi Indah, Jln Sgbesi Indah 3,
43300 Seri Kembangan Selangor

Date :



Signature of Supervisor: **Dr. S. Chandra Mohan**
Associate Professor
FASD

Name of Supervisor : **Universiti Teknologi PETRONAS**
Assoc. Prof Dr. Chandra Mohan

Date :

ACKNOWLEDGMENT

First and foremost, I would like to express my gratitude to Allah the Almighty, the one and only god, for without His consent; this study and thesis may not be complete. I would like to thank my wife, Nor Nadiah binti Ab Muntalib for her moral support, sacrifice and understanding throughout my study period. The same goes to my wonderful and friendly supervisor and co-supervisor, Assoc. Prof Dr. Chandra Mohan and Dr. Saravannan Karuppanan, I would like to thank both for all the advice and ideas given which help me to go through this phase. I also would like to apologize for any promise that have not been fulfilled, and any argument that we had during this period.

To all my friends in UTP, Mohd Rizal Lias, Modh Fahil Harfiez, and Mohd Fadzil Ali Ahmad, thank you for giving me support and thoughts towards the completion of this research. Although we have our argument in many subjects, we still share the same vision, to seek and knowledge for the sake of our younger generation. For my family, especially my mom, Ramlah binti Abdullah, thank you for the du', I love you mom.

I would like to remind myself to be a better person and researcher upon the completion of this study. I still have a long way to go. Do remember that the world is a place where you need to struggle learning, living, and helping others.

ABSTRACT

Fluidized bed has been used in wide applications due to its capability to provide a good mixing medium and heat transfer. It has been used and utilized for many processes in industrial scale on various applications such as catalytic cracking in the petroleum industry and gasification process in the energy industry.

The main focus of this work is to investigate a parameter for the fluidized bed operating in a bubbling regimes; the effect of different orifice shape on fluidization uniformity. For this purpose, Three (3) different orifice shapes were used, a classic straight drilled hole perforated plate (cylindrical), a nozzle like shape (nozzle), and also a diffuser like shape (diffuser). A numerical approach has been used to study the hydrodynamic as it is more cost saving while capable of producing a result which has a good agreement with the experiment results. A proper numerical validation was established using the data from the literature to ensure a workable simulation can be produce. The two fluid model (Eulerian-Eulerian) multiphase flow model coupled with the kinetic theory of granular flow was implemented in the simulation in predicting the pressure drop across the orifice plate as well as the bed expansion for all three (3) orifices. The particles dynamic in the bottom zone near the orifice plate was also investigated in order to have a clear view of the effect on the inlet velocity vector of using different orifice shape.

Based on the results obtained from the simulation, the diffuser and nozzle orifice shapes tend to give higher pressure drop compared to the cylindrical shape for the case of different number of orifices and different inlet velocity. However, the pressure drop across the orifice plate reduces with increasing number of orifices holes for all cases. For the bed expansion, all orifices shapes give the same trends where the average value taken from the bed shows the bed expands more vigorously with the increase of the inlet velocity.

The observation near the bottom zone depicts that at each orifices provide different results for different number of orifices cases. For the 13-orifice plate, the diffuser orifices show the most stable inlet velocity through the bed while for 19-orifice plate; nozzle orifice shows the most stable fluctuation. At a higher opening ratio, 39-orifice plate, both nozzle and diffuser orifices share the same trend where both of the orifices have a stable air distribution compared to the cylindrical orifice.

ABSTRAK

Fluidized bed telah digunakan untuk aplikasi yang berbeza kerana mempunyai kelebihan dari segi menyediakan percampuran sempurna dan pemindahan haba yang baik. Proses ini telah digunakan untuk pelbagai proses dari pelbagai sektor industri untuk aplikasi yang berbeza seperti pemecahan catalytic dalam industri petroleum dan juga proses gasifikasi dalam industry tenaga.

Fokus utama kajian ini dijalankan adalah untuk menyiasat satu faktor penting bagi fluidized bed yang beroperasi dalam rejim menggelegak ; iaitu kesan bentuk orifis yang berbeza pada keseragaman pembendaliran. Bagi tujuan ini, tiga (3) bentuk orifis yang berbeza telah digunakan , silinder, nozzle, dan juga diffuser. Satu pendekatan berangka telah digunakan untuk mengkaji hidrodinamik fluidized bed tersebut kerana ia menjimatkan kos dan mampu menghasilkan hasil yang sama dengan hasil eksperimen. Satu pengesahan berangka telah disimulasi dengan menggunakan data dari kajian yang lepas bagi memastikan satu model simulasi yang boleh digunakan dapat dihasilkan. Model dua bendalir (Euler - Euler), model aliran berbilang fasa ditambah pula dengan teori kinetik aliran berbutir telah digunakan pada simulasi untuk meramalkan penurunan tekanan merentasi plat orifis serta pengembangan fluidized bed untuk ketiga-tiga (3) orifis . Dinamik zarah dalam zon bahagian bawah dekat dengan plat orifis juga telah disiasat untuk mendapatkan pemahaman yang lebih jelas dari kesan perbezaan vektor halaju masuk menggunakan bentuk orifis yang berbeza.

Berdasarkan dari keputusan yang telah diperolehi daripada simulasi ini, Diffuser dan Nozzle orifis memberikan penurunan tekanan yang lebih tinggi berbanding dengan bentuk silinder lurus bagi kes orifis yang berbeza dan halaju masuk yang berbeza. Walau bagaimanapun, penurunan tekanan merentasi plat orifis berkurangan dengan peningkatan jumlah rongga lubang untuk semua kes. Untuk pengembangan katil, setiap bentuk orifis memberikan trend yang sama di mana nilai purata yang diambil dari katil menunjukkan katil berkembang dengan lebih tinggi

dengan peningkatan halaju masukan dan hanya kesan yang kecil dapat dilihat untuk bentuk orifis yang berbeza.

Pemerhatian berhampiran zon bahagian bawah menggambarkan bahawa setiap orifice memberikan hasil yang berbeza untuk setiap kes. Untuk plat 13-orifis, bentuk diffuser menunjukkan halaju masuk yang paling stabil melalui katil manakala bagi plat orifis 19; muncung orifis menunjukkan turun naik yang paling stabil. Pada nisbah lebih tinggi pembukaan, plat orifis 39, kedua-dua muncung dan peresap lubang berkongsi trend yang sama di mana kedua-dua dalam rongga badan yang mempunyai pengedaran udara yang stabil berbanding dengan orifis silinder.

In compliance with the terms of the Copyright Act 1987 and the IP Policy of the university, the copyright of this thesis has been reassigned by the author to the legal entity of the university,
Institute of Technology PETRONAS Sdn Bhd.

Due acknowledgement shall always be made of the use of any material contained in, or derived from, this thesis.

© Muhamad Hilme bin Ibrahim, 2013
Institute of Technology PETRONAS Sdn Bhd
All rights reserved.

TABLE OF CONTENTS

APPROVAL PAGE.....	ii
TITLE PAGE.....	iii
ACKNOWLEDGEMENTS	v
ABSTRAC.....	vi
ABSTRAK	viii
COPYRIGHT PAGE.....	x
LIST OF FIGURES	xiii
LIST OF TABLES.....	xvi
LIST OF ABBREVIATION.....	xvii
LIST OF NOMENCLATURE	xviii

1. INTRODUCTION

1.1 Gasification and Fluidization.....	1
1.1.1.1 Fluidization Regimes.....	2
1.2 Fluidized Bed Reactor.....	3
1.3 Geldard Classification of Particles.....	4
1.4 Computational Fluid Dynamics.....	6
1.5 Problem Statement.....	7
1.6 Problem State of the Art.....	8
1.7 Objectives.....	9
1.8 Scopes of Study.....	9

2. LITERATURE REVIEW

2.1 Bubbles Dynamics Theory.....	10
2.2 Experimental Approach.....	14
2.3 Numerical Approach.....	17
2.3.1 Lagrangian Approach.....	18
2.3.2 Eulerian Approach.....	20
2.4 Distributor Plate.....	24
2.4.1 Distributor Pressure Drop.....	26
2.5 Summary.....	28

3. METHODOLOGY

3.1	Simulation Set-up.....	30
3.1.1	Meshing / Grid Generation Study.....	31
3.1.2	Boundary Condition.....	32
3.1.3	Minimum Fluidization Velocity.....	32
3.1.4	Modeling Multiphase flow.....	34
3.1.5	Kinetic Theory of Granular Flow (KTGF).....	37
3.2	Distributor Plate.....	39
3.2.1	Cylindrical Orifice.....	39
3.2.2	Diffuser Orifice.....	39
3.2.3	Nozzle Orifice.....	41
3.3	Model Validation.....	41
3.4	Simulation Case.....	42

4. RESULTS AND DISCUSSION

4.1	Grid Independence Study.....	44
4.2	Hydrodynamics model Validation.....	45
4.3	Effect of Superficial Velocities to bubbling behaviour on different orifice shapes.....	48
4.3.1	Cylindrical orifice.....	48
4.3.2	Diffuser Orifice.....	54
4.3.3	Nozzle orifice.....	55
4.4	Effect of different Orifice shapes on the Distributor Pressure Drop	56
4.4.1	Distributor Pressure Drop for Different number of orifices.	56
4.4.2	Distributor Pressure Drop for Different Orifice Shapes.....	59
4.5	Effect of Different superficial Velocity on Bed Expansion.....	62
4.6	Effect of Different Jet Penetration Length on Different Orifice Shape.....	68

5. CONCLUSION AND RECOMMENDATION

5.1	Conclusion.....	71
5.2	Recommendation.....	72

REFERENCES.....	73
-----------------	----

LIST OF FIGURES

Figure 1.1: Fluidization regimes.....	3
Figure 1.2: Geldard Diagram.....	5
Figure 2.1: Patterns of bubble coalesce and solid circulation.....	11
Figure 2.2: Gas flow around the isolated bubbles with different bubble to U_{mf} ratio.....	13
Figure 2.3: Snapshot sequence in Fluidized bed.....	16
Figure 2.4: Dense phase streamlines surrounding a bubble taken from experiment and simulation.....	23
Figure 2.5: Variation of fluidization quality (Q) with aspect ratio for two (2) different multi-orifice distributors, A and B.....	25
Figure 3.1: Simulation Geometrical Model with Grid Generation.....	30
Figure 3.2: Cylindrical Orifice.....	40
Figure 3.3: Diffuser Orifice.....	40
Figure 3.4: Nozzle Orifice.....	40
Figure 3.2: Geometrical Model for validation.....	41
Figure 4.1: The velocity plot for different mesh interval used in the simulation...	45
Figure 4.2a: Comparison of the Bed Height simulation results with the experimental data from Busciglio et al. (2008).....	46
Figure 4.2b: Comparison of the Average Bed Height Simulation results with the experimental results from Busciglio <i>et al.</i> (2008).....	46
Figure 4.3.1a: Volume fraction contour at $1.33 U_{mf}$ for 13 cylindrical orifices.....	50
Figure 4.3.1b: Volume fraction contour at $2.00 U_{mf}$ for 13 cylindrical orifices.....	50
Figure 4.3.1c: Volume fraction contour at $2.67 U_{mf}$ for 13 cylindrical orifices.....	50

Figure 4.3.1d: Volume fraction contour at 1.33 U_{mf} for 19 cylindrical orifices.....	50
Figure 4.3.1e: Volume fraction contour at 2.00 U_{mf} for 19 cylindrical orifices.....	50
Figure 4.3.1f: Volume fraction contour at 2.67 U_{mf} for 19 cylindrical orifices.....	50
Figure 4.3.1g: Volume fraction contour at 1.33 U_{mf} for 39 cylindrical orifices.....	51
Figure 4.3.1h: Volume fraction contour at 2.00 U_{mf} for 39 cylindrical orifices.....	51
Figure 4.3.2i: Volume fraction contour at 2.67 U_{mf} for 39 cylindrical orifice.....	51
Figure 4.3.2a: Volume fraction contour at 1.33 U_{mf} for 13 diffuser orifices.....	51
Figure 4.3.2b: Volume fraction contour at 2.00 U_{mf} for 13 diffuser orifices.....	51
Figure 4.3.2c: Volume fraction contour at 2.67 U_{mf} for 13 diffuser orifices.....	51
Figure 4.3.2d: Volume fraction contour at 1.33 U_{mf} for 19 diffuser orifices.....	52
Figure 4.3.2e: Volume fraction contour at 2.00 U_{mf} for 19 diffuser orifices.....	52
Figure 4.3.2f: Volume fraction contour at 2.67 U_{mf} for 19 diffuser orifices.....	52
Figure 4.3.2g: Volume fraction contour at 1.33 U_{mf} for 39 diffuser orifices.....	52
Figure 4.3.2h: Volume fraction contour at 2.00 U_{mf} for 39 diffuser orifices.....	52
Figure 4.3.2i: Volume fraction contour at 2.67 U_{mf} for 39 diffuser orifices.....	52
Figure 4.3.3a: Volume fraction contour at 1.33 U_{mf} for 13 Nozzle orifices.....	52
Figure 4.3.3b: Volume fraction contour at 2.00 U_{mf} for 13 Nozzle orifices.....	53
Figure 4.3.3c: Volume fraction contour at 2.67 U_{mf} for 13 Nozzle orifices.....	53
Figure 4.3.3d: Volume fraction contour at 1.33 U_{mf} for 19 Nozzle orifices.....	53
Figure 4.3.3e: Volume fraction contour at 2.00 U_{mf} for 19 Nozzle orifices.....	53
Figure 4.3.3f: Volume fraction contour at 2.67 U_{mf} for 19 Nozzle orifices.....	53
Figure 4.3.3g: Volume fraction contour at 1.33 U_{mf} for 39 Nozzle orifices.....	54
Figure 4.3.3h: Volume fraction contour at 2.00 U_{mf} for 39 Nozzle orifices.....	54
Figure 4.3.3i: Volume fraction contour at 2.67 U_{mf} for 39 Nozzle orifices.....	54

Figure 4.4a: Average distributor pressure drop plots at different inlet velocities ratios for 13, 19, and 39 cylindrical orifices.....	57
Figure 4.4b: Average distributor pressure drop plots at different inlet velocities ratios for 13, 19, and 39 nozzle orifices.....	58
Figure 4.4c: Average distributor pressure drop plots at different inlet velocities ratios for 13, 19, and 39 diffuser orifices.....	58
Figure 4.4d: Average distributor pressure drop plots at different inlet velocities ratios for 13 orifices plate.....	60
Figure 4.4e: Average distributor pressure drop plots at different inlet velocities ratios for 19 orifices plate.....	60
Figure 4.4f: Average distributor pressure drop plots at different inlet velocities ratios for 39 orifices plate.....	61
Figure 4.5a: Average Bed expansion ratio at different velocity ratio for Diffuser orifice	63
Figure 4.5b: Average Bed expansion ratio at different velocity ratio for Nozzle orifice	63
Figure 4.5c: Average Bed expansion ratio at different velocity ratio for cylindrical orifice.....	64
Figure 4.5d: Average Bed expansion ratio at different velocity ratio for 13 orifices plate.....	66
Figure 4.5e: Average Bed expansion ratio at different velocity ratio for 19 orifices plate.....	67
Figure 4.5f: Average Bed expansion ratio at different velocity ratio for 39 orifices plate.....	67
Figure 4.6a: Air Velocity plot through the bed width taken at $1.67U_{mf}$, 0.01 m above the distributor plate for 13 numbers of orifices for Cylindrical, Diffuser, and Nozzle.....	69
Figure 4.6b: Air Velocity plot through the bed width taken at $1.67U_{mf}$, 0.01 m above the distributor plate for 19 numbers of orifices for Cylindrical, Diffuser, and Nozzle.....	69

Figure 4.6c: Air Velocity plot through the bed width taken at $1.67U_{mf}$, 0.01 m above the distributor plate for 39 numbers of orifices for Cylindrical, Diffuser, and Nozzle..... 70

LIST OF TABLES

Table 2.1: Summary of different experiments on hydrodynamics study.....	15
Table 2.2 Summary on the CFD-DEM approach simulation on Fluidized bed.....	19
Table 2.3: Summary on the Eulerian simulation.....	21-22
Table 2.4: Summary of study on distributor plate.....	24
Table 3.1: Simulation Model geometry.....	31
Table 3.2: Number of Grid Interval.....	32
Table 3.3: The Empirical Constants.....	33
Table 3.4: Parameter used for the validation.....	42
Table 3.5: Summary of all the orifice type and nos used in the simulation.....	42

LIST OF NOMENCLATURE

Letter

ΔP	: Pressure difference
P_s	: Granular pressure
L	: Length
u'	: Velocity fluctuation
A	: Area
d	: diameter
L	: Length
g	: Gravity
F	: Force
U_{mf}	: Minimum Fluidization Velocity
d	: Diameter
$C_{2,1}$: Empirical constant
C_{ds}	: Drag Coefficient
Ar	: Archimedes Number
Re	: Reynolds Number
N	: Number of Orifices

Greek Symbols

∇	: The Dell operator
π	: PI
ε	: Volume Fraction
\bar{v}	: Velocity
β_{gs}	: Drag Coefficient between gas and solid phase
Θ	: Granular Temperature
\bar{I}	: Interphase Momentum Exchange
$\bar{\tau}$: Stress tensor
γ	: Bulk Viscosity
g_o	: Radial distribution

μ : Viscosity
 μ_s : Granular Viscosity
 ρ : Density

Subscripts

g : gas
s : solid
p : particle
col : collisional
kin : kinetic
fric : friction

Abbreviations

2D : 2 Dimensional
CFD : Computational Fluid Dynamics
FVM : Finite Volume Method
KTGF : Kinetic Theory of granular Flow

CHAPTER 1

INTRODUCTION

1.1 Gasification and Fluidization

Combustion is one of the oldest methods used to extract energy from any solid or liquid carbon based substances, e.g. fossil fuels. However it is known that the fossil fuels combustion has increased the carbon dioxide (CO₂) content in the atmosphere. In 2005, the CO₂ concentration was increased approximately 180-300 ppm more than the equilibrium concentration for the last 650 000 years (N.H Florin, *et al.*, 2008). The CO₂ build-up in the atmosphere will increase the climate temperature as CO₂ is one the greenhouse gases. Therefore, the alternative processes capable to replace this oldest method which can produce lower emission are enticing more attention in the recent decades.

Gasification is one of the alternative methods which capable to replace combustion process. It has advantages on the environmental impact where it emits a non-hazardous by products compared to the conventional direct combustion. Gasification is a process of converting a fossil fuel based carbonaceous materials to a synthesis gas with a usable heating value. The definition has excluded combustion because the product, flue gas, does not contain any heating value (Chris Higman *et al.*, 2003).

The process occurred in a bed or reactor namely gasifier with controlled amount of oxidant (air, oxygen, and/or steam). One of the most commonly used gasifier in the gasification process is fluidized bed. The fluidization method has been applied for the purpose of gasifying the feedstock and has been applied widely in several process

involving gasification, pyrolysis, and combustion for wide range of particulate materials involving biomass thanks to their great mixing capabilities and transfer properties (S. S. Sadaka *et al.*, D.A. Nemstoy *et al.*, V.Tanneura *et al.*, 2002, 2008, 2008).

Fluidization occurs when granular solid particles resemble fluid motions. It occurs when air or gases flow through the interstices of particles exerting a drag force on the particle. At a certain velocity, namely the minimum fluidization velocity, the fluid drag will have sufficient force to support the weight of the particles and counteract the gravitational force thus making the particles to float and behave like a fluid. The quality of the fluidization is affected by several factors such as; the size and distribution of the particles, the gas to solid ratio, the geometry of the fluidization vessel, gas inlet arrangements, and the mixing of particles in the reactor.

Fluidized bed is widely used in the petrochemical industry. The reactor is used for various applications such as catalytic cracking of petroleum where large petroleum molecules were cracked into smaller molecules, acetone recovery where acetone is recovered from the air, and coal gasification where synthesis gas such as Hydrogen and Carbon Monoxide was produced from a gasification process, and many other processes.

1.1.1 Fluidized Regime

In fluidization process, different regimes can occupy in the same reactor during any processes. These regimes exist and can swiftly change from one to another by manipulating the inlet velocity which is introduced into the bed. These regimes can be categorized into five (5) different regimes; packed bed (fixed), bubbling bed, turbulent bed, fast fluidization bed, and pneumatic transport regime. At relatively low velocity, namely superficial velocity, the drag force exerted by the gas is merely insufficient to overcome the gravitational force of the particles thus the gas percolates through the void between the particles. This regime is known as a *packed bed* or fixed bed regime.

Increasing the superficial velocity will give the particles enough force by the gas to counterbalance the gravitational force and the bed start to behave like a pseudo liquid. At this point, the superficial velocity is known as minimum fluidizing velocity. Further increase of the velocity will expand the bed and the bubbles will start to form after the superficial velocity exceeds another characteristic value called minimum bubbling velocity (P. Basu, 2006). This regime is known as *bubbling bed* regime.

Further increase of the velocity will cause bubbles to coalesce forming a larger bubble which is called slug. This is known as a turbulent regime. A further increase in the fluid flow and an efficient entrained solid transport enable the bed to be operated in the fast fluidization method. At higher fluid flow, the solid particles are pneumatically conveyed outside the bed. This regime is known as pneumatic transport regime. Figure 1.1 below depicts the regimes of fluidization, starting from fixed bed to the pneumatic conveying.

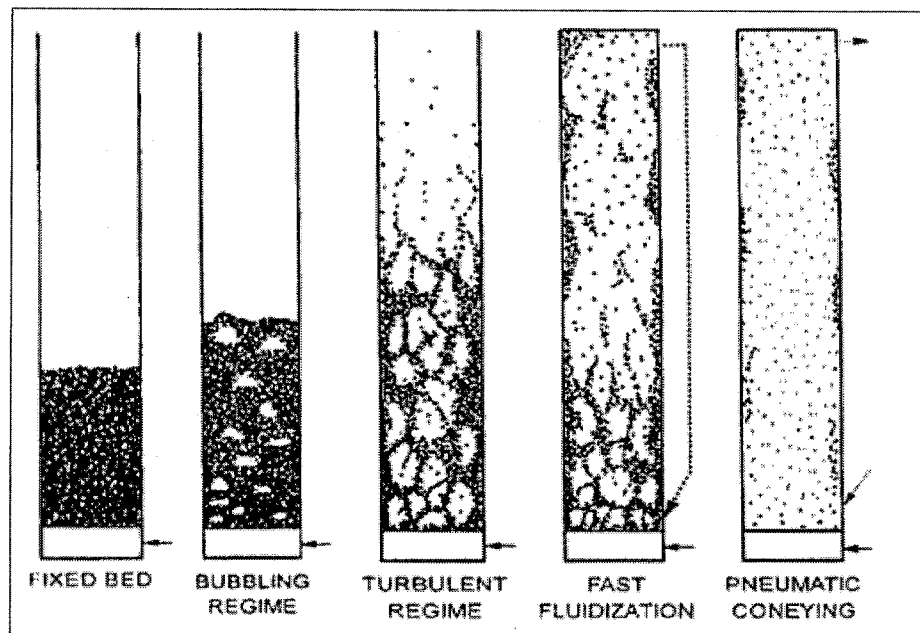


Figure 1.1: Fluidization regimes

1.2 Fluidized bed reactor

Fluidized bed reactor consist of three (3) important parts; a plenum chamber, orifice plate (distributor plate), and a container. Plenum chamber is responsible to collect the inlet air before entering the reactor which is located at the bottom of the reactor. The compressible air from the compressor or blower will be collected before purging in through the orifice plate above it before reacting with the particles inside the container.

Container is the largest part of the reactor where it holds and contains the particles, gas/air, or liquid while the reactions take places during the process. Several regions exist during the fluidization process in the container where the bottom area occupied by the particles is known as the bed region and the free area is known as the freeboard. Most of the containers were designed to be cylindrical shape where it does not contain any rough edges which can disturb the mixing in any processes.

The orifice plate is intended to distribute the inlet air into the bed region in the container while supporting the bed weight. It is considered being the most important part in the reactor due to its effect to the fluidization stability. The orifice plate can be broadly categorized into three (3) groups (P. Basu, 2006).

- i. Porous or straight-hole orifice type. Usually punched or vertically drilled through a plate or sintered plate.
- ii. Nozzle type or bubble cap type which is used to distributed air through downward holes.
- iii. Sparge pipe type which consists of air carrying tubes with a number of holes punctured through the tubes.

1.3 Geldard Classification of Particles

According to Geldard, the fluidization technique can be applied only with specific particles. The particle behavior in a gas-solid fluidized bed under ambient conditions mainly depends on the particle diameter and density. In 1973, Geldard classified particles into four groups, A, B, C and D, according to their behavior (D. Geldard, 1973).

The particles are categorized into four (4) groups as depicted in Figure 1.2. These particles are;

- i. Geldard A particles have size range between 20 -100 μm and density of 1400 kg/m^3 . The particles in this group fluidized easily.
- ii. Geldard B particles have size range between 40-500 μm and density of 1400-4500 kg/m^3 . The particle in this group give a less stable bed formation compared to the group A particle.
- iii. Geldard C particles have mean size $<30 \mu\text{m}$ and low density. The particles in this group are hard to fluidize and they give a non-uniform fluidization.
- iv. Geldard D particles have size greater than 600 μm and have high density. Higher density requires high minimum fluidization velocity to fluidize the bed. The particles in this group usually form larger bubbles compared to the particles in group A and B.

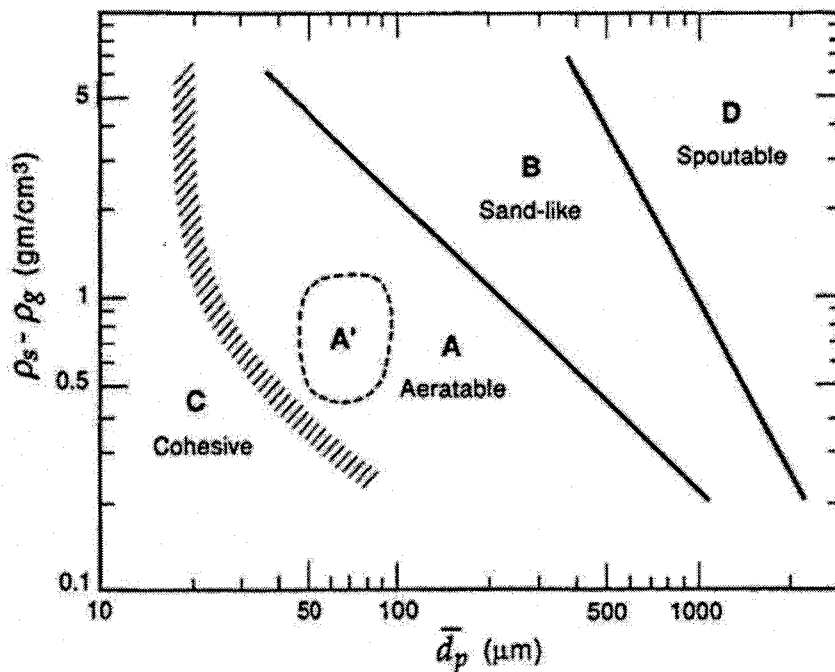


Figure 1.2: Geldard Diagram (D. Geldard, 1973).

1.4 Computational Fluid Dynamics

Computational Fluid Dynamics (CFD) is computer software that uses algorithm and numerical method to calculate and solve problems related to fluid flow and heat transfer. Using numerical analysis as its core, the software implements finite volume, finite element, or finite element method as a discretization method to solve the partial differential equations. This discretization method is a way to convert or change the continuous partial differential equation such as Navier-Stoke Equation and Euler Equation to discrete difference equation.

The most common used discretization technique in CFD is finite volume method (FVM). In FVM, the divergence theorem were used to transform the volume integral in a Partial Deferential Equation (PDF) which contain a divergence term to the surface integral which then are evaluated as flux. The flux flow in FVM is conserve and identical, from one control volume to the adjacent control volume. The FVM also have the ability to be formulated for the unstructured meshing on the geometry.

There are three (3) main steps in solving any simulation using the CFD code, pre-processing stage, simulation, and as well as post-processing stage.

i. Pre-processing stage

In the preprocessing, the geometry of the problem will be modeled and defined. The model will then be divided into small grid or discrete cells through a meshing process. The meshing process is one of the most important steps in the CFD simulation since the size and type of the mesh used will govern the accuracy of the entire simulation process. Besides meshing, all the physical modeling and the fluid properties will be defined at this stage, for example the equation of motion, momentum, and energy equation. Boundary conditions which define the boundary of the geometry will be defined in this stage.

ii. Simulation

The simulation stage is where the computer will compute the iteration according to the earlier selection in the preprocessing stage. The simulation will solve the equation as a steady or transient state problem depending on the user definition on solving the problem.

iii. Post-processing

In this stage, all the required graph and data can be analyzed and visualized according to the user requirement.

CFD is one of the most important tools for engineer to help them understand the process and visualize certain effect on their equipment and machines. It has many advantages where it is considered to be extrusive method, where the observation of flow can be obtained without disturbing the flow itself. It also can provide observation of flow properties at locations which may not be accessible to the measuring instruments. CFD are also used as a qualitative tool to narrow down and or selecting design in an early design stage.

1.6 Problem Statement

The most concerned parameters in the bubbling fluidized bed is the bubbles formation owing its direct implication on fluidization efficiency and stability. A large number of small diameter size bubbles are required to have a stable fluidization in the bubbling regime. In general, there are two (2) different aspects which contribute to the bubble formation, the dynamics parts which are related to the inlet velocity, air viscosity, particle diameters and the reactor geometry which are related more to the physical geometry of the reactor such as bed diameter, bed height, and the orifice plate type.

The importance of the orifice plate can be clearly seen by its function on supporting the bed materials and distributing or channeling the flow to the bed materials. In fact there are no other physical means beyond the orifice plate which influence the air distribution

through the solid phase proving how critical the orifice plate to the bubbling fluidized bed. The effectiveness of different orifice plate is measured by the resistivity where a high resistance orifice is desirable due to its ability to sustain a uniform bubbling. Higher grid resistance compared to the fluctuation in pressure drop can dampen the total bed pressure drop and grid pressure drop (D. Geldard, 1973). Both the stability and efficiency of a process in the bubbling fluidized bed reactor depends directly on the uniform air distribution.

Most current perforated type orifice plate give a non-uniform fluidization and back shifting of solid materials into the plenum chamber which can reduce the effectiveness of the entire process. This problem may arise due to the conventional shape and arrangement used in the most perforated orifice plate which give a low pressure drop or low resistivity. The arrangement of the orifice can also be considered to be a factor which results in the non-uniformity of the fluidization.

Different shape of orifice can be used to replace the conventional shape as long as it can produce a better resistance and giving higher pressure drop which can minimize the non-uniformity and back shifting of solid. This study will be focused on the orifice shape for its effect on the pressure drop and the uniformity of the fluidization. Owing to the advance in the computer modeling nowadays, a numerical approach is used as it can reduce the cost for the fabrication of the experimental setup and can produce similar result with good agreements with the experimental data.

1.7 Current State of the Art

This research is inspired when the student was attached for a Gasification Project funded by Universiti Teknologi Petronas (UTP) and Tenaga Nasional Berhad Research Sdn Bhd (TNBR) to develop a 150kW gasification pilot plan. The pilot plant is operate using a bubbling fluidized bed method for three (3) number of feedstock's as fuels. The fluidization however did not give any satisfying result that may cause by various factors.

The distribution plate or orifice plate may be one of the reasons for poor gasification and bubbling as the distribution plate have a significant impact on the fluidization process. A few distribution plate were designed and use in the gasification based on different arrangement but continue to use the same shape which is a straight drilled hole. The research is intended to look into a new perspective of manipulating the shape and the opening ratio instead of focusing on the configuration.

1.8 Objective

The main objective of this study is to investigate different orifice shape to the hydrodynamic of bubbling fluidized bed. The sub-objective of this research can be summarized in the following

- i. To investigate different inlet velocity effect on the uniformity of fluidization.
- ii. To study the effect of different orifice shapes on the uniformity of fluidization

1.8 Scope of Study

The study will concentrate on three (3) different distribution plates which have different orifice shape experimentally and numerically using CFD code, FLUENT® version 14. A two dimensional (2D) domain will be used for simulation with the dimension is fixed to 0.8 m Height x 0.2 m Length. The plenum chamber is model to be rectangular in shape with height equivalent to 0.075 m and the orifice plate has a constant 0.005 m of thickness.

The particles used in for all the simulations are belonging into Geldard B particle with a constant density of 2650 kg/m^3 and the inlet air was introduced at a room temperature with a constant density of 1.177 kg/m^3

CHAPTER 2

LITERATURE REVIEW

The hydrodynamics of the bubbling fluidized bed (BFB) can be considered as a complex and chaotic process since it deals with a multiphase condition. This complexity and chaotic behavior arises from the rapid interaction of inter-particles and air-particles through mixing and segregation as well as due to rising and interacting bubbles (Schout, Van den Bleek, 1992; Shouten *et al.*, 1996). Most of the previous studies done on the hydrodynamics of an BFB reactor are focused on the formation of bubbles and its properties and some studies focused on the bed geometry and design with an objective of improving the quality and efficiency of the process.

Before going further in this research, the mechanism and behavior of bubbles need to be fully understood as it has a significant effect on the stability and effectiveness of the fluidization process. In this chapter, different theories of the bubbles will be introduced in order to provide a clear and complete picture on the theory behind all the experimental and numerical studies done that previously done. The literature review will then be presented for both experimental and the numerical studies by previous researchers on the hydrodynamics of BFB.

2.1 Bubble Dynamics theory

Winkler (1922) defined bubbles in the fluidized bed as large, rising voids resulting from the flow instabilities that occur due to the flow around the bed materials. The bubbles formed just above the minimum fluidizing velocity or higher for a certain type of particle and its occurrence is purely random (Yates *et al.*, 1994). The bubbles are often referred to exhibit similar behavior as real bubbles in liquid with a similar spherical capped shape (Yates *et al.*, Swarbrick J. *et al.*, 1994, 1992).

The bubbles are also governed by different forces depending on the gas inlet flow rate. At a very low flow rate, the frequency and the size of the bubbles are primarily governed by a balance between the surface tension of the fluid and the buoyancy force of the bubbles and at a higher flow rate, the inertia of the liquid moved by the rising bubbles become more apparent (Swarbrick J. *et al.*, 1992).

Instead of travelling in a perfect vertical direction, the bubbles in the fluidized bed move upwards in irregular trajectories with small aberration along the vertical line. This aberration occurs due to the presence of obstacles in terms of other bubbles, or presence of directed flow particles towards the bubbles path resulting from a different pressure gradient at certain regions in the bed. As the bubbles rise to the bed interphase from the bottom of the reactor, the size of the bubbles increases mainly due to coalescence with other bubbles in both vertical and horizontal directions (Yates *et al.*, Swarbrick J. *et al.*, 1994, 1992) and due to the lower hydrostatic pressure at the top of fluidized bed (Swarbrick J. *et al.*, 1992). Joshua Drake (2011) has drawn patterns of the bubbles coalesce and circulation for two parameters; increasing bed height with a constant gas velocity and increasing of gas velocity with a constant bed height shown in Figure 2.1.

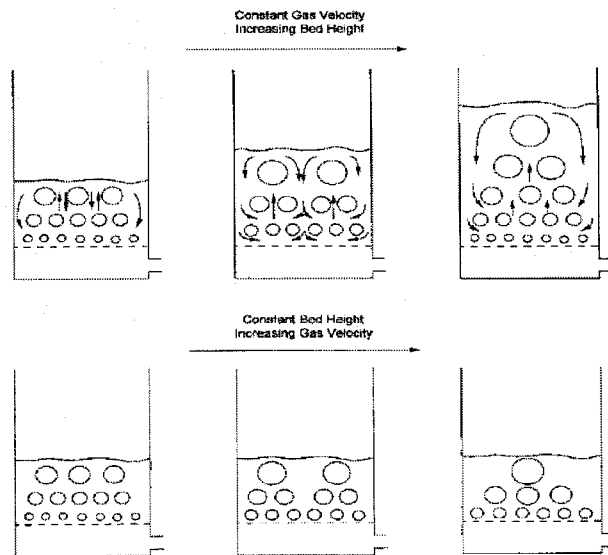


Figure 2.1: Patterns of bubble coalesce and solid circulation (Joshua Drake, 2011)

The theoretical study was performed for a better understanding of the bubble dynamics and hydrodynamics of the bed in general. The theoretical models were developed based on experimental observations. Different researchers have proposed different theories on the formation of bubbles, its occurrence, and discovered the factors which contributed to its features and behaviors. Toomey and Johnstone (1952) proposed a two-phase theory with the assumptions that the fluidization consists of two (2) distinguish regions; bubble and emulsion phase. The bubbles were produced when the introduced air flow were in excess of the required flow to fluidized the bed. This two-phase model is in fact the most established model where few other models were developed based on it such as Davidson-Harrison (1963) and Kunii-Levenspiel model (1966).

Davidson-Harrison (1963) had managed to develop a simple theory on the bubble formation which is capable to explain many phenomena that have been observed experimentally. The model predicts the existence of spherical surface with zero velocity, called a cloud. The model has the following assumptions;

- i. The particulate phase is an incompressible fluid with a bulk density similar to that of a fluidized bed at minimum fluidization.
- ii. The relative velocity between the particles and the fluidizing medium is assumed to be proportional to the pressure gradient within the fluid, and thus Darcy's law is applicable.
- iii. Fluidizing fluid is assumed to be incompressible.
- iv. The pressure throughout the bubble is constant.
- v. The particulate phase behaves as an inviscid liquid.
- vi. The bubble has a circular cross section.

The model has a correlation between the stream geometry and bubble velocity, U_B . The term fast bubble and slow bubble in this model refers to the bubble velocity relative to the minimum fluidization velocity where in slow bubble case, $U_B < U_{mf}$ and for the fast bubble case, $U_B > U_{mf}$. Figure 2.2 illustrates different streamline geometry acting upon the bubble at various velocity ratios; fast bubble, slow bubble, and very fast bubble velocity.

Kunii and Levenspiel (1966) developed a theory based on two-phase model and Davidson-Harrison (1963) bubble model. The cloud phase which had been identified in the Davidson-Harrison (1963) model is considered to be a separate phase in this model. For the wake phase, the model assumed the wake concentration is equal to the solid concentration in the emulsion phase and the average velocity of solid and gas in the wake region is assumed to be equal to the upward velocity of the bubbles.

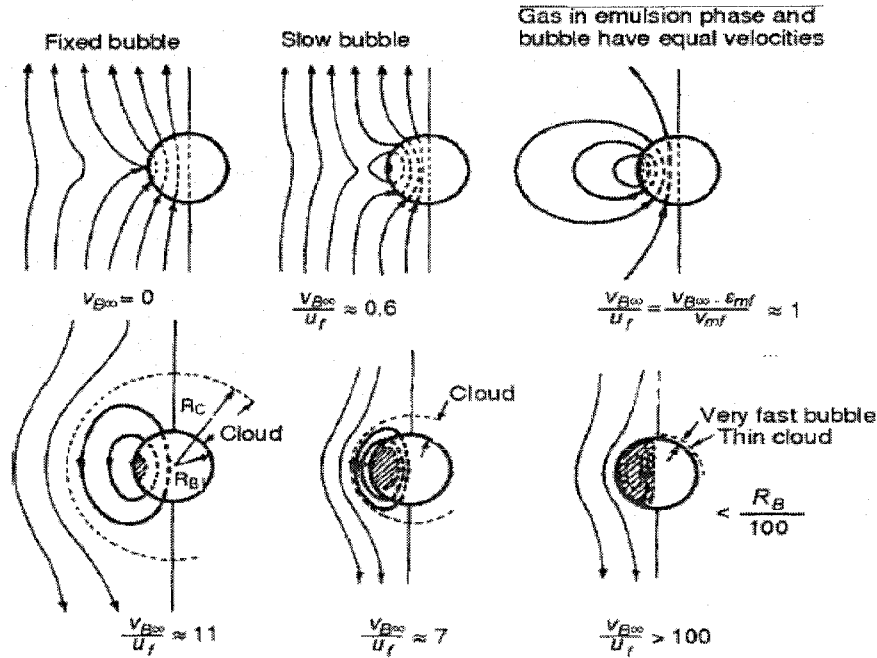


Figure 2.2: Gas flow around the isolated bubbles with different bubble to U_{mf} ratio [7]

Besides Davidson-Harrison (1963), and Kunii-Levenspiel (1966), there are many theoretical models on bubbles developed and studied over the time by different researchers. Partridge and Rowe (1966) model was studied and reviewed by Ellis *et al.* (1968) and Chavarie and Grace (1975). The comparisons on those models were also investigated by Chavarie and Grace (1975) for a catalytic decomposition of ozone in two-dimensional fluidized bed. From the study, out of the four models tested based on two-phase theory, Kunii-Levenspiel (1966) model gave the best overall representation of the experimental data.

2.2 Experimental Approach

Experiments in the field of multiphase flow of fluidized bed have been conducted over the last centuries to corroborate existing correlations and existing theoretical models on the fluidization hydrodynamics. These experimental studies on the BFB hydrodynamics are normally focused on several important parameters such as; void fraction and solid concentration, bubble size distribution and rise velocity, and liquid-solid phase velocities (Athirah *et al.*,2010) . The advancement in the field of measurement has enabled the researchers to utilize all the measurement equipment to help them to understand more on the fluidization hydrodynamics.

Measurement technique generally can be divided into two categories; intrusive and non-intrusive. Intrusive technique is used for a local measurement where it provides a point measurement in a volume. Intrusive equipment has a direct contact with the flow field and it is usually embedded into the reactor. Some examples of the intrusive equipment that are normally used are pressure transducer, capacitance probe, and temperature probe.

On the other hand, non-intrusive technique is used for a global measurement which it provides an average value for the parameters, e.g. a phase fraction within 2D and 3D spaces. The examples of non-intrusive measurement equipment are Particle Image Velocimetry (PIV), Digital Image Analysis (DIA), Laser Doppler Anemometry (LDA) and etc.

Each of the technique discuss above were choose and implemented based on the studied parameters of the hydrodynamics. Table 2.1 summarizes few experiments done to measure the hydrodynamics properties by implementing different techniques and equipment's.

Author	Parameters	Objectives/Findings
Volker Wiesendorf <i>et al.</i> (2000)	Capacitance Probe CFB	<ul style="list-style-type: none"> • CP was used to measure the solid volume concentration and solid velocity near the dilute region. • The capacitance probe technique is a powerful tool for flow structure investigations even under the harsh conditions of industrial fluidized-bed reactors
Mengxi Liu <i>et al.</i> (2011)	Intrusive method - Optical Probe Non-intrusive method - Pressure Probe	<ul style="list-style-type: none"> • Comparison of the bubble size captured by optical probe (non-intrusive), pressure probe (intrusive) and theoretical bubble size by Horio Nonaka (1987). • Optical probe tend to overestimate the bubble chord length due to its inability to measure small bubbles. • Pressure probe readings were analyzed using pressure analysis and IOP analysis where the IOP analyses give similar trends with Horio & Nonaka (1987).
Antonio Busciglio <i>et al.</i> (2008)	Digital Image Analysis (DIA)	<ul style="list-style-type: none"> • Implementing the DIA technique to measure the bubble properties using two velocimetry techniques; Eulerian Velocimetry techniques (EVT) and Lagrangian Velocimetry techniques (LVT). • The data give promising results to fully characterize the complex dynamic behavior of bubbles and also it can be used for CFD validation in post processing.
Gaurav Agarwal <i>et al.</i> (2011)	Particle Image Velocimetry (PIV) With DIA	<ul style="list-style-type: none"> • PIV was used to measure the motion of particles and jets in the grid-zone region of a fluidized bed to develop a grid zone phenomenological model and quantify the effects of fluidization velocity, orifice diameter, orifice pitch, particle diameter, and particle density on grid zone characteristics. • Jet diameters are a function of orifice velocity and diameter. • Jet length increases with the increase of jet velocity.

Table 2.1: Summary of different experiments on hydrodynamics study

Volker Wiesendorf *et al.* (2000) investigated the solid volume concentration and velocities in the upper dilute zone of a cold circulating fluidized bed (CFB) and in the bottom zone of a CFB boiler using a Capacitance Probe (CP) which is an intrusive technique. He had found that the CP Technique is capable to provide a measurement for the volume concentration and velocities under a harsh environment.

For the non-intrusive method, the advantages in the Digital Image Analysis (DIA) technique have been proven useful in the field of fluid dynamics where Antonio Busciglio *et al.* (2008) and Caicedo *et al.* (2003) used this technique in their study. Antonio Busciglio *et al.* (2008) used the DIA to measure bubble properties i.e bubble size, bubble velocity, hold-ups and bed heights by using in-house image analysis method. The experimental results obtained were in agreement with the relevant literature correlation. The snapshot sample from the DIA technique is presented in figure 2.3. Caicedo *et al.* (2003) also implemented DIA technique to measure the bubble properties. The bubble size and aspect ratio effect with different inlet velocity was investigated. From the study, he found that the bubble size and aspect ratio follow a normal distribution with the decrease of inlet velocity.

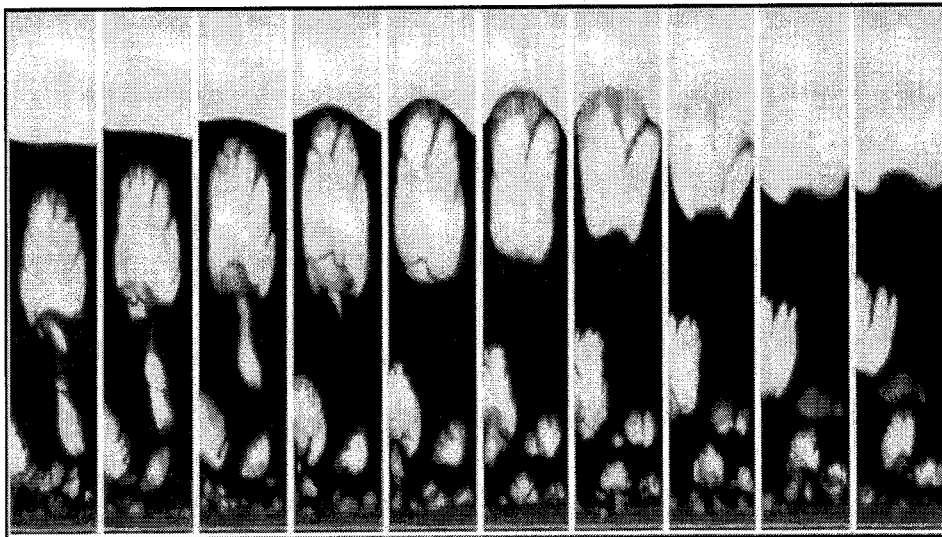


Figure 2.3: Snapshot sequence in Fluidized bed (Antonio Busciglio *et al.*, 2008)

Guarav Agrawal (2011) and I Julian *et al.* (2012) in the recent study combined two (2) non-invasive techniques, DIA and PIV, to measure and analyze the bubble and fluidization particle properties. The coupling technique gives more advantages in terms of the experiment capability to measure different types of parameters. The coupling techniques of PIV and DIA have shown the effects of operating variables on the particle movement and the bubble flow characteristic and the experiments have provided valuable information to be taken into accounts in the reactor design.

2.3 Numerical Approach

Computational fluid dynamics (CFD) has been implemented for many years in solving both simple and complicated engineering problems which require a physical observation which is not possible to be captured or modeled using experiments. The advancement of the multiphase flow in the CFD model provides more opportunities to researcher and engineers to explore and solve more problems involving multiphase reaction.

The multiphase flow field can be modeled using two frame of reference or approaches; Lagrangian and Eulerian frame. The approaches are based on the description on the motion of fluids and its associated properties. In Eulerian approach, the fluid motion is observed at a fixed location, where the properties are captured as different material pass through the location. While in the Lagrangian approach, the observer follows the fluid particle and measures the fluid properties through the flow field. For each category, there are several more different models available which are suitable for different types of problems.

The multiphase of fluidization process can be divided into two (2) different phase; continuum and disperse phases. The dispersed phase represents the solid fuels or the sand particles in the bed while the continuum phase represents the air or gas inlet. The fluidization process has been successfully simulated by different researchers using CFD code using both approaches; Eulerian and Eulerian-Lagrangian approach. These simulations are capable to model the bubbling and mixing behavior in of fluidized bed.

In the Eulerian-Lagrangian approach, many researchers have used the combination of CFD and Discrete Element Method (DEM) model in their simulations. In DEM, the granular material is treated as rigid particles where the inter particle interaction is explicitly considered. The first application reported in literature using the DEM-CFD approach was in plug flow of solid in horizontal pipe by Tsuji *et al.* (1992). From that day, the DEM-CFD couplings are broadly used in the simulation of many problems involving multiphase condition.

2.3.1 Lagrangian Approach

In the Lagrangian-Eulerian (LE) approach for the BFB, the model tracks all the dynamic movement of the solid individually, while the air phase is treated as continuum. In the LE approach, interphase transfer of mass, momentum and energy are represented by coupling terms that appear in the Eulerian conservation equations for the fluid phase. (Shankar Subramaniam, 2013).

B.H. Xu *et al.* (1997) have successfully modeled a CFD-DEM coupling method for an Eulerian-Lagrangian fluidized bed. The CFD-DEM model is shown to be capable to produce realistic dynamic information on the fluidized bed at different level from the overall process to the individual particle. The CFD-DEM coupling could also be very useful in elucidating the mechanism governing the fluid-solid two-phase flow and in studying the complex phenomena in a flow system in a cost effective way.

Falah Alobaid *et al.* (2013) has brought the CFD-DEM to another level by extend the model where additional grid, called particle grid in which the physical value for the solid particles will be calculated. The usual approach for the model is both the solid particle and continuum physics were solved in the continuum grid due to larger area. From the study, the CFD-DEM shows a high qualitative correlation on the particle distribution in the bed and quantitative agreement on the pressure gradient at different positions on the side wall of the bed. However, this model has risen the computational time extremely.

The summary of the numerical studies using this approach for the fluidized bed is shown in Table 2.2

Author	Parameters	Objectives/Findings
B.H. Xu, A. B. Yu (1997)	Fluidized Bed	<ul style="list-style-type: none"> • Successfully implemented the DPM-CFD to model the gas solid flow in fluidized bed. • Used Newton's second law to solve the properties of individual particles and Navier-Stoke for the gas flow.
K.D. Kafuia, <i>et al.</i> (2002)	Minimum fluidization velocity	<ul style="list-style-type: none"> • To provide two novels coupling method from the Eulerian-Lagrangian point on view to measure the minimum fluidization velocity, Pressure gradient form (PGF) and buoyancy force based on fluid density. • Both methods have shown a good agreement with the empirical correlations and pressure drop-velocity profiles with PGF give the most consistent results with empirical results.
Alberto Di Renzo, <i>et al.</i> (2007)	Bed expansion and minimum fluidization velocity	<ul style="list-style-type: none"> • Investigation of the hydrodynamic properties of liquid-solid fluidization and gas-solid fluidization (without cohesive force). • The expansion regime and bed surface rising velocity has been found to be in good agreement with the propagation velocity of kinematic shock for the liquid fluidization. • The gas fluidization had shown that the minimum fluidization velocity give a similar value to the experimental observation and theoretical predictions.
Maryam Karimi <i>et al.</i> (2012)	Pressure fluctuation analysis	<ul style="list-style-type: none"> • To determine the compatibility of CFD-DEM with the experimental data of fluidized bed. • Used S-statistic and wavelet transform (WT) as a new approach in comparing the fluidization hydrodynamics with the experimental data. The pressure fluctuations of various frequencies were used to do the comparison. • S-statistic which is a state space domain pressure fluctuation analysis was applied to both simulation model and experimental data showing that they share a similar dynamic mechanism.

Table 2.2 Summary on the CFD-DEM approach simulation on Fluidized bed

2.3.2 Eulerian Approach

The other approach of simulating the bubbling fluidized bed is by implementing Eulerian-Eulerian Multiphase model. The model is preferred for simulating macroscopic hydrodynamics (C.C. Pain *et al.*, 2001). The Eulerian-Eulerian or Two Fluid model treats both the continuum and disperse phase in the fluidized bed as interpenetrating continua, where the volume of a phase could not be occupied by other. The theory of inter-penetrating continua is built upon the conception that allows multiple velocities in the same spatial location at the same time. In this approach, a drag model is implemented to solve the interaction between these two (2) phases.

Eulerian with Kinetic theory of granular flow

Kinetic Theory of Granular flow is a model incorporated to the particulate phase in Eu-Eu model. The theory is basically an extension of the classical kinetic theory of gases to dense particle flow, which provides explicit closures that take energy dissipation due to non-ideal particle-particle collisions into account by means of the coefficient of restitution. The models predicted well the bubble formation, time-averaged and instantaneous velocities of particle and gas phases, and volume fraction in the gas bubbling fluidized beds as reported in many studies.

B.G.M. Van Wachem *et al.* (1999) in his study focused on validating the Eulerian-Eulerian model applied to freely bubbling fluidized bed by comparing with the trends predicted by empirical correlation and experimental data. The simulation was compared with the Baskakov *et al.* (1986) theory on the fluctuation of pressure where the simulation is in good agreement with the theory especially at a higher gas velocity. The simulation result also reflects the behavior for the Kolmogorov entropy which quantifies the unpredictability of chaotic system in which the author conclude that the Eulerian CFD simulations could be useful scale up tools. Other similar researches using the Eulerian-Eulerian are summarized in Table 2.3.

Author	Parameters	Objectives/Findings
A. Samual Berg <i>et al.</i> (1996)	Circulating fluidized bed Axial particle velocity	<ul style="list-style-type: none"> • Studied the radial profile of axial particle velocity. • The model predicts a core annulus flow which is similar to the experiment results and only depicted an over prediction on the down-flow velocity near the bed wall.
B.G.M. Van Wachem <i>et al.</i> (1998)	CFX code Bubble size	<ul style="list-style-type: none"> • Studied the different bubble sizes at different velocities. • Compared the simulation model with theoretical models. (Darton (1977) for bubble diameter vs. the height and Hilligardt and Werther (1986)) • Predicted bubbles size is in agreement with the theoretical model.
Li. Huilin <i>et al.</i> (2003)	Particle distribution Particle interaction	<ul style="list-style-type: none"> • Studied the motion of particles with the binary mixture. • Hydrodynamics of gas related to the particle size distribution and interaction between particles. • Effects of particle size distribution are needed to be taken into account in the modeling of the fluidized bed as the parameters are important.
K. Johnson <i>et al.</i> (2006)	CFX Stress model Air Feed System	<ul style="list-style-type: none"> • Compared two (2) different particle rheology model; constant particle viscosity (CPV) and KTGF. • KTGF model gives a more evenly distributed bubble flow profile over the bed cross-section, while the CPV model gives a more parabolic bubble flow profile, with a higher bubble flow in the central part of the bed. • KTGF model results are significantly in better agreement with the experiments. It is furthermore shown that the modeling of the air-feed system is crucial for predicting the overall bed dynamic behavior.
Liang Yu <i>et al.</i> (2006)	Gas composition KTGF and Chemical kinetics	<ul style="list-style-type: none"> • Used two fluids models, KTGF and chemical reaction kinetics, to predict the impact of flow on chemical reaction and to determine the distribution of pressure, velocity, and volume fraction and exit gas composition. • Calculated gas composition gives a good agreement with the experimental data.
Li. Huilin <i>et al.</i> (2007)	Different particle density and size	<ul style="list-style-type: none"> • Studied the flow behavior of mixing and segregation in bed. • Larger and heavier particles tend to settle down at the bed and better mixing is obtained by increasing the fluidization velocity.

Table 2.3: Summary on the Eulerian simulation

Author	Parameters	Objectives/Findings
Antonio Busciglio <i>et al.</i> (2009)	Bubble properties CFX code	<ul style="list-style-type: none"> Investigated the bubble properties (bed expansion, bubble hold up, size evolution, density, distribution, aspect ratio, and bubble velocimetry). For the bed expansion, the CFD value is in acceptable with the experimental data with a slight underestimation for a low velocities model. For the other parameters, the simulations give a generally acceptable agreement with the experimental data
Mahdi Hamzehei (2011)	Particle diameter Superficial velocity	<ul style="list-style-type: none"> Studied the effect of particle diameter and superficial gas velocity to the bed hydrodynamics. Compared the simulation with the experimental data on pressure drop and time averaged bed depicted a good agreement. Small bubbles are produced at the bottom of the bed and collided when they move upwards.
Jingyuan Sun <i>et al.</i> (2011)	Bubble and particle dynamic behavior	<ul style="list-style-type: none"> Simulated the bubble and low density polyethylene particle dynamic behavior in gas-solid fluidization. The model was validated by pressure fluctuation experiments The multi-fluid model is capable to compute two kinds of particle turbulent kinetic energies, laminar granular temperature due to random individual particle oscillation and turbulent granular temperature.
F.Hernandez-Jimenez <i>et al.</i> (2011)	Dense phase velocity Drag Model	<ul style="list-style-type: none"> Studied the time-averaged horizontal and vertical component of the dense-phase velocity and the drag function. The Gidaspow Drag Model gives the most similar result to the experimental data <u>with an exception to the bubble probability parameter.</u>
Athirah Mohd Tamidi <i>et al.</i> (2011)	Inlet medium Bed parameters Particle size	<ul style="list-style-type: none"> Studied the effect of air and steam medium to different particle size and the effect of initial bed height to the hydrodynamics of the reactor. Certain ranges of particle size can give an optimum fluidization of the particles and the initial bed height does not give any significant improvement on the fluidization in the gasifier.

Table 2.3: Summary on the Eulerian simulation

K. Johnson *et al.* (2006) in his research dig further on the closure model on the TFM used to close the set of equation. He compared two (2) different particle rheology model; constant particle viscosity (CPV) and KTGF model with the experimental data using a cold bubbling fluidized bed operating in a slugging regime. He found that the PSD distribution from the simulations employing the constant particle viscosity (CPV) provide a narrower and higher amplitude peaks indicating higher regularity of the pressure fluctuation while the PSD distribution in the simulation using the kinetic theory of granular flow (KTGF) approach in combination with high maximum packing is in a good agreement with the experimental result.

F. Hernandez *et al.* (2011) in his study compared two fluid model simulations and the Particle Image Velocimetry (PIV) for a two-dimensional gas-solid fluidized bed. The comparison image is shown in Figure 2.4 below. From the comparison, he concluded that TFM able to quantitatively predict the bubble growth and velocity as well as the bubble probability distribution within the bed. However, the time averaged velocity taken for the dense phase does not provide the same observation as the bubble phase where TFM overestimate the value compared to the experimental result.

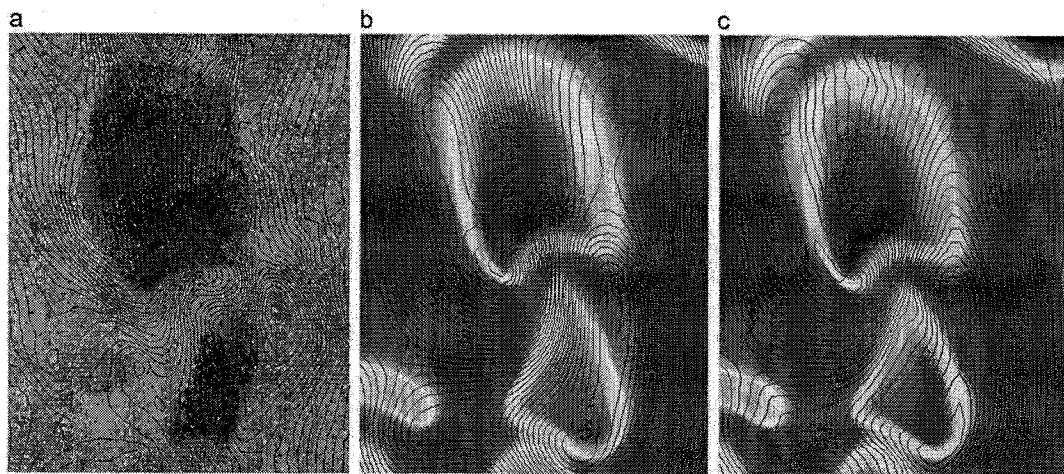


Figure 2.4 ; Dense phase streamlines surrounding a bubble taken from experiments (a), and simulation (b), also included the simulation results with the streamlines incorporating the dense phase velocities inside bubbles (c). The simulation and experimental results are, respectively, shown superimposed to their particle volume fraction map and image of particles (F. Hernandez *et al.*, 2011)

2.4 Distributor plate

Even though there are many numerical studies which are focused on the bubbling of fluidized bed, there are only few studies in literature focusing on the effect of distributor plate on the bubbling or incorporated the distributor plate in their simulation.

Author	Parameters	Objectives/Findings
Wei-Ming Lu <i>et al.</i> (1999)	Feed rate, gas flow rate, opening ratio, hole diameter Pressure fluctuation	<ul style="list-style-type: none"> Stability of fluidized bed is determined by the plate design, feed rate, and gas velocity profile through the plate hole. Formation of a suspension bed can be categorized into three (3) stages, induced, growing and stable stage. The plate with the small opening ratio holds more suspended particles and builds a suspension bed at a lower minimum suspension velocity. The plate with the large opening ratio can operate over a wide range of operational variables, including the gas flow, feed rate etc.
D.Sathiyamoorthy, Masayuki Horia (2003)	Model equation Aspect ratio, distributor plate	<ul style="list-style-type: none"> Distributor type, aspect ratio, and operating velocity influence the quality of fluidization. Distributor plates affect the shallow bed remarkably.
Frédéric Depypere <i>et al.</i> (2004)	CFD Simulation Pressure drop Wire mesh distributor	<ul style="list-style-type: none"> CFD model revealed the inhomogeneous air flow towards the distribution plate was due to lateral air inlet. The air distribution was more uniformly formed when using bottom air inlet instead of side inlet.
Gaurav Agarwal (2011)	PIV, DIA Jet penetration above the distributor plate	<ul style="list-style-type: none"> Jet diameter is only a function of orifice velocity and diameter. Jet penetration length decrease with the increase of particle density, particle diameter, and orifice pitch. Higher orifice pitch distributor plates tend to have early transitional state.

Table 2.4: Summary of study on distributor plate

Table 2.4 summarized some of the study done on the distributor plate from both the experiments and numerical approach. Wie-Ming Lu *et al.* (2009) used both simulation and experimental approach to study the effect of fluidization stability using a perforated type distributor with two different opening ratios. From his study, he concluded that the distributor plate design is one of the factors contributing to the fluidization stability.

D. Sathiyamoohy *et al.* (2003) focused on the mathematical modeling which relates the distributor plate type as well as operating velocity. Two (2) distributor plates with different opening ratios were used in the experiment. The ratio of distributor to bed pressure drop has been expressed as a function of aspect ratio and compared to the literature data. Figure 2.5 depicts the difference of the fluidization quality of two (2) different multi orifice distributor used in the experiments. The fluidization quality is observed to be different for both cases.

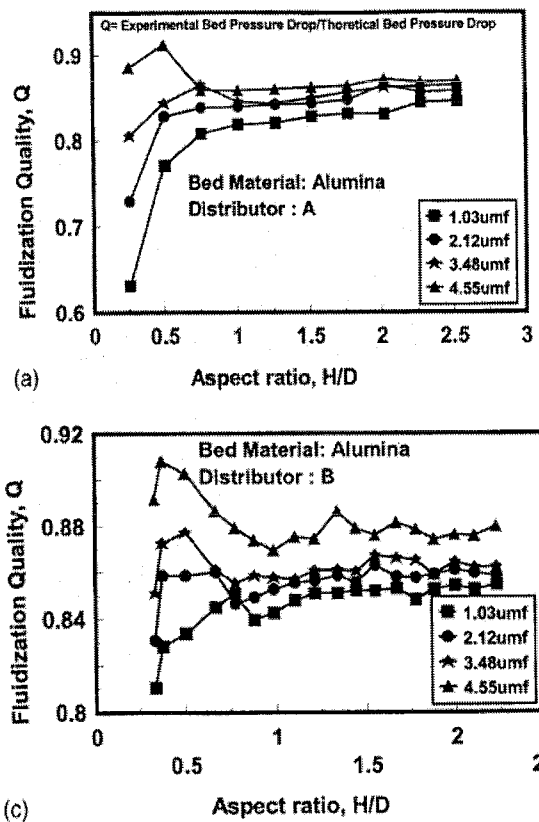


Figure 2.5: Variation of fluidization quality (Q) with aspect ratio for two (2) different multi-orifice distributor, A and B.

Gaurav Argawal *et al.* (2011) in his paper focused on the jetting phenomena in the grid zone region; a region above the distributor plate. In order to understand the motion of particles and jet, different bed media and different type of distributor plates were used. Figure 2.5 depicts the maximum moving zone diameter versus orifice velocity for different distributor plate. It can be observed that different distributor plate giving different results orifice velocity.

M.T. Dhotre *et al.* (2007) study the effect of opening area and orifice diameter in a range of 0.64 to 4% and 2-4mm respectively using a two fluid model for a three dimension cold model. He found out that the chamber configuration has an effect on uniformity of gas distribution particularly in the sparger region of bubble column reactor. He concluded in his study that the uniformity of gas distribution was found to increase with an increase of gas distributor pressure drop and a decrease in kinetic head of the gas.

2.4.1 Distributor Pressure Drop

Achieving a uniform air distribution is important to ensure uniform bubble formatting through the bed. Gas distributor or distributor plate is responsible to distribute the air from the plenum chamber through the container. A good distributor plate is measure by following qualities;

- i. Low pressure drop at operating velocity to minimize power usage
- ii. Have a high material properties to withstand thermal and mechanical stress
- iii. Able to prevent particle backflow to the plenum chamber
- iv. Able to prevent erosion due to particle collision

Having a high pressure drop is important to provide a uniform air distribution although low pressure drop are favorable to minimize the power usage. Having a low pressure drop will cause non-uniform air distribution as the air will flow through the lowest pressure drop created above the plate. Botterill *et al.* (1982) considered distributor plate pressure drop have a significant influences on the uniform and stable bed fluidization.

A conventional bed design considered the ratio of the distributor pressure drop over the bed pressure drop, usually nominated as R. The ratio is different for the shallow and deep bed. A bed is considered as shallow when the static bed height is less or equal to the bed diameter and it is considered to be deep when the length of static bed height is higher than the length of bed diameter.

The pressure ratio is influenced by several parameters such as distributor type, Geldart Particle used in the fluidization, bed depth, superficial gas velocity, bed diameter and etc. Agarwal *et al.* (1962) recommended a minimum value of 0.1 for R ratio for a deep bed while for a shallow bed, minimum pressure drop of 350mm of water is recommended.

Saxena *et al.* (1979) conducted an experiment using a 2D square bed of 305mm x 305mm using two different distributor types; porous plate and conical bubble cap type. He observed that R ratio value at minimum fluidization depends on the bed height and the value increases rapidly with increase in fluidization velocity. It is also found that the distributor pressure drop decreases with the increase of percentage open area and is independent of the bed weight or height for a given distributor design. Smaller bubble size for a high pressure drop distributor plate over a lower pressure drop was reported in the study.

Different researchers have used different distributors in their study, mostly to improve the design. Different types of distributor; multi orifice type, perforated plate type, bubble cap type, stand pipe type and etc were studied with respect to its hydrodynamic properties. The research also takes into account the geometrical properties; orifices size, spacing or orifice pitch position, orientation and solid backflow.

Chyang and Hyang *et al.* (1991) investigated the behavior of pressure drop across a perforated plate distributor with and without the bed medium. A higher distributor pressure drop was observed in the bed with the bed medium compared with the empty bed at low bed velocity and the pressure was significantly affected by the locations of pressure taps corresponding to the orifice layout on the perforated plate.

Sh. Saberi *et al.* (1995) conducted an experiment using a cylindrical bed with 0.286m diameter and 1m height using 8 tuyeres plates with different number of orifices. From the study, it is found that the pressure drop increase with the increase of superficial velocity to the bed and the main source of resistance to the gas flow is caused by the contraction at the exit nozzle.

Celia sobriano (2009) investigated the effect of two different distributor types, bubble cap and perforated plate type which then compared with the theoretical estimation. She have found the different distributor plate have a significant effect on the bed hydrodynamics where the perforated plate distributor having a higher pressure drop compared to the bubble cap type.

Gaurav Argawal *et al.* (2011) is his paper studied the evolution of inlet gas jets located at the distributor by varying the distributor types and bed media to understand the motion of Particles and jet formation at a near gear zone region. From the experiment, he found that the jet diameters were depend on the orifice velocity and orifice diameter and jet penetration length was found to increase with the orifice velocity and orifice diameter and decrease with increase in particle diameter, density, and orifice pitch.

J.M Paiva *et al.* (2004) investigated the dynamics of the bottom zone of a fluidized bed using a cold model of 0.1 diameter and 1.3m height by using six different perforation plates, a metallic mesh, and a porous ceramic. The result indicated that the flow changes with the operating condition.

2.5 Summary

Both literatures on experimental and numerical have been presented in this chapter. Overall, most of the experimental studies on hydrodynamic can produce fantastic results and capable to measure all the hydrodynamic properties. However, there are constraints in experimental study. Using an intrusive equipment can only provide limited results and the presence of the equipment itself will definitely affect the process thus providing misleading result. Although using a non-intrusive technique may solve the problem, each of the non-intrusive equipment have a limited capability and needed to be used or

with another equipment in order to studies wider parameters. For this reason, simulation studies seem more reliable and cost effective in studying the hydrodynamics of the BFB. The experimental studies are time consuming in terms of setup the test rigs and the equipment calibration.

In numerical work, both Lagrangian-Eulerian and Eulerian-Eulerian multiphase flow model for the CFD were presented where both of the multiphase models are capable to provide a good simulation for the BFB hydrodynamics. Lagrangian-Eulerian approach can be efficiently use if the volume fraction for the discrete phase is small otherwise the approach is no longer applicable as it will be very expensive in terms of computational time. For this study, The Eulerian-Eulerian approach method is favorable in modeling the bubbling fluidization because it consumes lower computational time and able to provide results which are in good agreement with experimental data.

CHAPTER 3

METHODOLOGY

3.1 Simulation Set-up

In this study, a CFD code, ANSYS Fluent 6 has been utilized to simulate the hydrodynamics in the Gas-solid Bubbling Fluidized Bed (BFB). The cold reactor model was drawn and meshed using Gambit version 2.3.16 software and then imported to Fluent for the processing and post processing. The model was drawn in the 2-Dimensional plane (x-y plane) as shown in Figure 3.1 below;

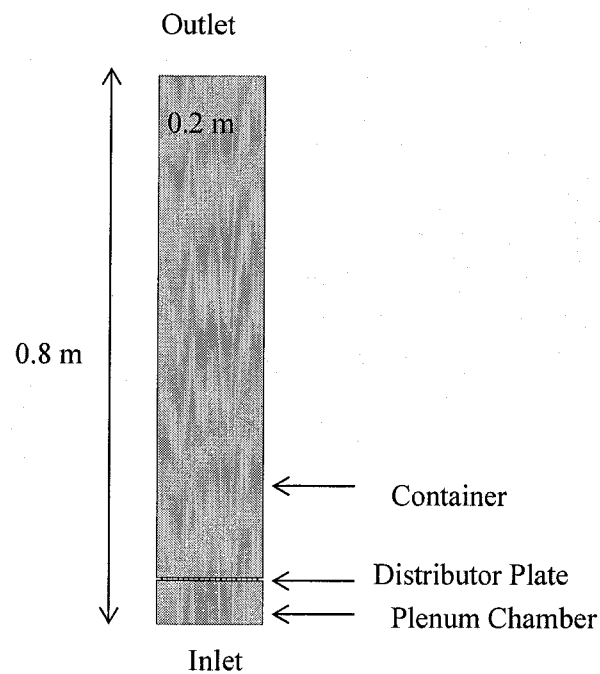


Figure 3.1: Simulation Geometrical Model with Grid Generation

Dimension	Unit (mm)
Height	800
Plenum Chamber Height	75
Bed Diameter	200
Orifice Plate Thickness	5

Table 3.1: Simulation Model geometry

The model consists of three (3) main components; plenum chamber, distributor plate, and container. The components dimension is shown in the Table 3.1. The meshing and the boundary condition for the model were pre-applied in the Gambit software and the properties for the boundary condition were then re-defined in the Fluent Software. The Eulerian-Eulerian multiphase flow coupled with KTGF is then applied as well as the drag model.

3.1.1 Meshing / Grid Generation Study

Meshing is one of the most important factors in simulation that needs to be examined carefully. The only goal of meshing or grid generation is to transform the complex physical domain to a simpler triangular or rectangular domain on which the crucial boundary condition may be accurately approximated. (C. J. Chen *et. al*, 2000)

The meshing process is a process of dividing the model into small and discrete element called grid. It is a discrete representative of the geometry where the governing equation will be solved inside each of the portions of the domain. The grid generation should be done in such a way to attain all the following objectives;

- i. To minimize the numerical error
- ii. To provide a numerical stability
- iii. To provide computational economy

In this grid generation study, few grid sizes were generating using Gambit software. The interval size of the grid used shown in Figure 3.2.

Interval	No of Cells
0.005	17,398
0.004	37,994
0.003	45,146
0.002	108,402

Table 3.2: Number of Grid Interval

3.1.2 Boundary Condition

Choosing or implementing the right boundary condition is significant in solving the Navier-Stoke and continuity equation. It is important because it directs the motion of flow and specifies flux into the computational domain. The inlet and outlet boundary conditions used in the 2-dimensional model are:

- Inlet velocity boundary condition is used to define the velocity vector and scalar at the inlet boundary.
- Outlet pressure boundary condition is used to define the static pressure at flow outlets.
- Wall with no slip boundary condition is used to define the fluidized bed's wall.

3.1.3 Minimum Fluidized Velocity

Minimum fluidized velocity is the lowest velocity required to fluidize a bed and transform the fluidization regime from a packed bed to a bubbling bed regime which have been explained thoroughly in Chapter 1. The minimum fluidized velocity is obtained by solving two (2) equations, the Ergun equation for the packed bed and the drag equation within the bed. The Ergun equation correlates the bed pressure drop per unit height for a uniform particle diameter, d_p and is given by;

$$\frac{\Delta P}{L} = 150 \frac{(1-\varepsilon)^2}{\varepsilon^3} \frac{\mu U}{\phi d_p^2} + 1.75 \frac{(1-\varepsilon) \rho_g U^2}{\varepsilon^2 \phi d_p} \quad (3.1)$$

While the fluid drags equation is given by;

$$F_D = \Delta PA = AL(1 - \varepsilon)(\rho_p - \rho_g)g \quad (3.2)$$

The uniform fluidization velocity is calculated using equation (3.3) where C_1 and C_2 are the empirical constants from experiments. The assumptions used in the equation are

- i. The particles are in the perfect sphere shape
- ii. All the particles have the same size
- iii. The viscosity and air density was taken at the room temperature

There are several empirical constant values from the experiments. Table 3.3 summarizes different values of C_1 and C_2 .

Table 3.3: The Empirical Constants

Researcher	C_1 value	C_2 value
Wen and Yu	33.7	0.0408
Richardson	25.7	0.0365
Saxena and Vogel	25.3	0.0571
Babu et al.	25.3	0.0651
Grace	27.2	0.0408
Chitester et al.	28.7	0.0494

In this study, the U_{mf} was calculated using the value from Grace. The U_{mf} is calculated using the particle Reynolds's number

$$Re_{mf} = \frac{U_{mf}d_p\rho_g}{\mu} = [C_1^2 + C_2Ar]^{0.5} - C_1 \quad (3.3)$$

Where Ar is the Archimedes number given by

$$Ar = \frac{\rho_g(\rho_p - \rho_g)gd_p^3}{\mu^2} \quad (3.4)$$

3.1.4 Modeling Multiphase flow

Multiphase flow and frame of reference has been explained generally in the previous Chapter. As this study has implemented CFD code Fluent to simulate the problem, in this sub-chapter, a detailed and thorough explanation will be covered for the multiphase model that were choose to simulate the bubbling in the BFB.

In Eulerian–Eulerian approach (Eu-Eu) , all the phases present in the simulation are treated as a continuum base, where the model solves sets of momentum and continuity equations for each phase There are several available models in the Fluent code for Eulerian-Eulerian (Eu-Eu) approach; Volume of fluid (VOF), Mixture, Eulerian. Each of the models is developed for a different type of multiphase flow.

Based on the available multiphase model, Eulerian model or Two Phase Model (TPM) was preferred to simulate the bubbling behavior in a fluidized bed. Few assumptions need to be made in order to have a complete momentum balance. The assumptions are listed below;

- i. A single pressure is shared by both phases
- ii. Frictional viscosity is neglected in the simulation
- iii. The system operates in a Laminar flow
- iv. Solid phase shear stress, bulk viscosity, solid phase pressure gradient were obtained using KTGF.

The Eulerian model, like other multiphase model need to solve several equations related to scalar continuity equation, mass and momentum balance equations.

Continuity Equation

The continuity equation can be written for each phase as:

$$\frac{\partial}{\partial t} (\epsilon_g \rho_g) + \nabla \cdot (\epsilon_g \rho_g \vec{V}_g) = 0 \quad (3.5)$$

$$\frac{\partial}{\partial t} (\epsilon_s \rho_s) + \nabla \cdot (\epsilon_s \rho_s \vec{V}_s) = 0 \quad (3.6)$$

$$\varepsilon_g + \varepsilon_s = 1 \quad (3.7)$$

Momentum Equations

The momentum balance equations for each phase are derived based on the assumption that there is no mass transfer between the two phases, no lift or external body force and virtually no mass force acting on the secondary phase of the system. The momentum balance equations for each phase are listed as follows;

Gas phase momentum equation;

$$\frac{\partial}{\partial t} (\varepsilon_g \rho_g \bar{u}_g) + \nabla \cdot (\varepsilon_g \rho_g \bar{u}_g \bar{u}_g) = -\varepsilon_g \nabla P + \nabla \cdot \bar{\tau}_g + \varepsilon_g \rho_g \vec{g} + \beta_{gs} (\vec{v}_g - \vec{v}_s) \quad (3.8)$$

The gas phase stress tensor is equation 3.8 is given by;

$$\bar{\tau}_g = \varepsilon_g \mu_g \left(\nabla \vec{v}_g + (\nabla \vec{v}_g)^T \right) + \varepsilon_g \left(\lambda_g + \frac{2}{3} \mu_g \right) \nabla \cdot \vec{v}_g \bar{I} \quad (3.9)$$

Solid phase momentum equation;

$$\begin{aligned} \frac{\partial}{\partial t} (\varepsilon_s \rho_s \bar{u}_s) + \nabla \cdot (\varepsilon_s \rho_s \bar{u}_s \bar{u}_s) = \\ -\varepsilon_s \nabla \rho_g - \nabla P_s + \nabla \cdot \bar{\tau}_s + \varepsilon_s \rho_s \vec{g} + \beta_{gs} (\vec{v}_s - \vec{v}_g) \end{aligned} \quad (3.10)$$

Where, P_s is the granular pressure, $\bar{\tau}_s$ is the solid stress tensor which can be expressed as:

$$\bar{\tau}_s = \varepsilon_s \mu_s \left(\nabla \vec{v}_s + (\nabla \vec{v}_s)^T \right) + \varepsilon_s \left(\lambda_s + \frac{2}{3} \mu_s \right) \nabla \cdot \vec{v}_s \bar{I} \quad (3.11)$$

The interphase momentum defined in the KTGF and standard drag models are used to estimate the momentum exchange between phases

$$\beta_{gs} (\vec{v}_s - \vec{v}_g) = \varepsilon_s \nabla P_g - F_g \quad (3.12)$$

The momentum changes between the phases can be further described by Gidaspow drag function as follow;

For $\varepsilon_g > 0.8$

$$F_g = \frac{3}{4} \frac{\varepsilon_s \varepsilon_g \rho_g}{d_p} C_{ds} [\vec{v}_s - \vec{v}_g] \varepsilon_s^{-2.63} \quad (3.13)$$

For $\varepsilon_g < 0.8$

$$F_g = 150 \frac{\varepsilon_s (1 - \varepsilon_s) \mu_g}{\varepsilon_s d_p^2} + 1.75 \frac{\rho_g \varepsilon_g |\vec{v}_s - \vec{v}_g|}{d_p} \quad (3.14)$$

Where

$$C_{ds} = \frac{24}{\varepsilon_s} [1 + 0.15 (\varepsilon_g Re_s)^{0.687}] \quad (3.15)$$

$$Re_s = \frac{\rho_g d_p |\vec{v}_s - \vec{v}_g|}{\mu_g} \quad (3.16)$$

Solid pressure is composed of the kinetic term and term due to particle collision (ANSYS User guide). The solid pressure will be calculated independently when the volume fraction is lower than the maximum allowed fraction.

$$P_s = \varepsilon_s \rho_s \Theta_s + 2P_s (1 + e) \varepsilon_s^2 g_o \Theta_s \quad (3.17)$$

Radial distribution function is a modification of the probability of collision between particles.

$$g_o = \left[1 - \left(\frac{\varepsilon_{st}}{\varepsilon_{st,max}} \right)^{1/3} \right]^{-1} + \frac{1}{2} d_s \sum_{k=1}^N \frac{\varepsilon_k}{d_k} \quad (3.18)$$

Granular viscosity is the summation of three viscosity contribution namely, the collisional, kinetic, and frictional viscosity and can be represented as

$$\mu_s = \mu_{col} + \mu_{kin} + \mu_{fric} \quad (3.19)$$

The collision viscosity is a viscosity arises due to collision between particles. Its algebraic equation is taken from the kinetic theory of granular flow by Lun *et al.* (1984) which expressed the collisional viscosity as follow;

$$\mu_{\text{col}} = \frac{4}{3} \epsilon_s \rho_s d_p g_0 (1 + e_s) \left(\frac{\theta_s}{\pi} \right)^{0.5} \quad (3.20)$$

The Gidaspow *et.al* model is based on kinetic theory of gas where it assumed that the particles in the dilute region do not collide and both the restitution coefficient and radial distribution is equal to 1.

$$\mu_{\text{kin}} = \frac{2\mu_{\text{dil}}}{g_0(1-e)} \left[1 + \frac{4}{5} (1 + e) \epsilon_s g_0 \right]^2 \quad (3.21)$$

The frictional viscosity is contribution of the friction between particles and the total shear stress. When the solid volume fraction approaches the maximum packing limit, the rubbing and friction effect will be the main effect between the particles.

$$\mu_{\text{fric}} = \frac{P_{s,\text{fric}} \sin \beta}{2\sqrt{I_{2D}}} \quad (3.22)$$

Granular bulk viscosity can be defined as the granular particles resistance to compression or expansion and the model is developed from kinetic theory of granular flow (Lun *et. al*, 1984)

$$\lambda_s = \frac{4}{3} \epsilon_s \rho_s d_p g_0 (1 + e_s) \frac{\theta_s}{\pi} \quad (3.23)$$

3.1.5 Kinetic Theory of Granular Flow (KTGF)

Kinetic Theory of Granular Flow (KTGF) is developed from a Kinetic Theory of non-uniform gas. It is used to describe the kinematics found in granular media in an Eulerian-Eulerian multiphase model (Justin A. Grant *et. al*, 2006), i.e., the particulate

phase viscosity and particulate phase pressure gradient in the momentum Equation 3.10 above. The model calculates the solid phase stresses using Granular Temperature concept, where the random particle motion is linked to the thermal motion of molecules in a gas [60].

The granular temperature is a function of solid stress and defined based on solid fluctuation velocity of u' as,

$$\Theta = \frac{1}{3} u'^2 \quad (3.12)$$

The differential transport equation for granular temperature, describing the particle velocity fluctuation by a separate conservation equation can be written as;

$$\frac{3}{2} \left[\frac{\partial}{\partial t} (\varepsilon_s \rho_s \Theta_s) + \nabla \cdot (\varepsilon_s \rho_s \vec{u}_s \Theta_s) \right] = (-p_s \bar{\bar{\tau}}_s) : \nabla \vec{V}_s - \nabla \cdot q_s - \gamma_\Theta - 3\beta_{gs} \Theta \quad (3.13)$$

The terms of the equation above can be explained by:

Transient term + Convective term = Energy Generation by Solid phase stress + Flux of Fluctuation Energy – collision energy dissipation + exchange energy term with gas phase

The partial Differential Equation for the granular temperature was usually simplified to an algebraic equation by neglecting the convection and diffusion terms because of assumption in a dense, slow moving fluidized bed, local generation and dissipation of granular temperature far outweigh the transport by convection and diffusion [61]. The term is reduced to

$$0 =: \nabla \vec{V}_s - \gamma_\Theta \quad (3.14)$$

Collisional Energy Dissipation

The collisional dissipation term represent the dissipation of granular energy due to inelastic particle-particle collision and expressed by the model of Lun *et al.* (1984) as below;

$$\gamma_{\theta_s} = \frac{12(1-e_s^2)\rho_s g_0}{d_s \sqrt{\pi}} \epsilon_s^2 \theta_s^{3/2} \quad (3.15)$$

Dissipation term take into account the particle-particle coefficient of restitution which represent by the e_s in Equation 3.15 above. The coefficient of restitution is a fraction of energy dissipated due to inelastic collision of particles which varies from 0 to 1, which 1 for fully elastic collision without loss of energy and vice versa.

3.2 Distributor Plate

Perforated plate distributor commonly used owing to its simplicity and easy to fabricate compared to the other type of distributor. In this study, distributors based on perforated principle were used to investigate different geometrical effect on the hydrodynamics of fluidization. The perforated plates used in this study are differing in terms of the orifice shapes and the numbers on the distributor plate.

3.2.1 Cylindrical orifice

A cylindrical based is commonly used in any simulation study. It is also known as a straight drilled holes orifice. It has the same diameter on the top and bottom of orifice plate and normally used due to its simplicity; easy to fabricate. Figure 3.2 below depicts the geometry of the cylindrical orifices.

3.2.2 Diffuser Orifice

A diffuser shape orifice is actually a conical shape which have different diameter on the top and bottom of plate. It has a larger diameter on the top side and smaller diameter at the bottom of the plate. Figure 3.3 depicts the 3-D view of the diffuser orifice.

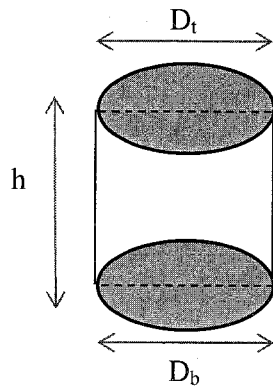


Figure 3.2: Cylindrical Orifice

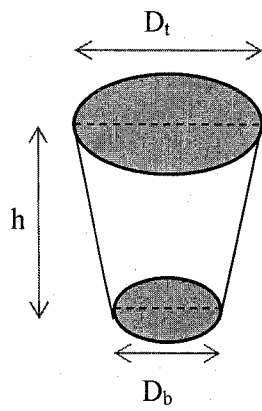


Figure 3.3: Diffuser Orifice

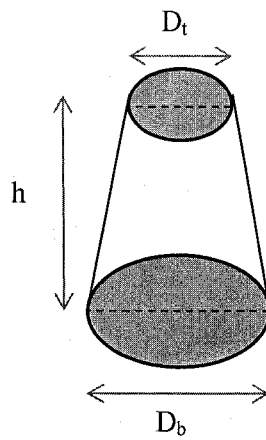


Figure 3.4: Nozzle Orifice

3.2.3 Nozzle Orifice

Nozzle orifice has an exact geometry as the diffuser orifice and differs only on the orientation. It has a small diameter at the top and larger diameter sit at the bottom of the plate resembling a nozzle cone shape. The nozzle orifice shape is depicted in Figure 3.4.

3.3 Model Validation

The model was validated using Busciglio *et al.* (2008) results. The geometrical model and parameters used for the validation shown in Figure 3.2 and table 3.5 below;

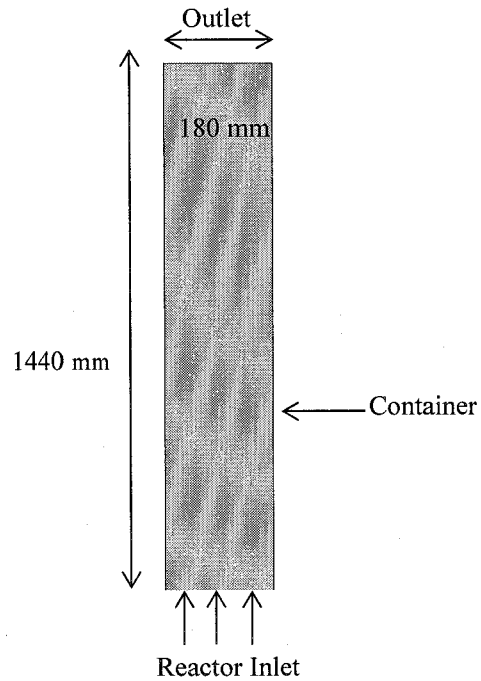


Figure 3.2: Geometrical Model for validation

Property	Value	Remarks
Solid Density	2500 kg/m ³	Glass Ballotani
Solid particle diameter	231µm	Fixed
Solid Viscosity	1.72 x 10 ⁻³ kg/m.s	Constant
Air Density	1.225 kg/m ³	Air
Air viscosity	1.7894 x 10 ⁻³ kg/m.s	Constant
Superficial Gas velocity	0.0891 m/s	Constant
Restitution Coefficient	0.9	Busciglio et al, 2009
Initial Solid Packing	0.65	Busciglio et al, 2009
Maximum Solid Packing	0.8	Fixed
Static Bed Height	360mm	Constant
Bed Width	180mm	Constant

Table 3.5: Parameter used for the validation

3.4 Simulation Cases

Table 3.4 below depicts all nine cases run through the simulation for all three orifices, cylindrical, diffuser, and nozzle shape.

No	Orifice Geometry	Top Orifices Diameter, Dt (mm)	Bottom Orifices Diameter, Db (mm)	Distance between orifices (mm)	No of Orifices	Opening %
1	Cylindrical	2	2	0.015	13	10.21
2	Cylindrical	2	2	0.01	19	14.92
3	Cylindrical	2	2	0.005	39	30.63
4	Diffuser	2	1	0.015	13	10.21
5	Diffuser	2	1	0.01	19	14.92
6	Diffuser	2	1	0.005	39	30.63
7	Nozzle	1	2	0.015	13	5.10
8	Nozzle	1	2	0.01	19	7.46
9	Nozzle	1	2	0.005	39	15.31

Table 3.4: Summary of all the orifice type and orifices number used in the simulation

The opening area ratio is calculated based on the total number of opening on the distributor plate over the total area.

$$\text{Total area of opening} = N \times (\pi d^2/4) / (\text{Plate Area})$$

$$\text{Percentage area of opening} = N \times (\pi d^2/4) / (\text{Plate Area}) \times 100$$

The distance between the orifices was calculated from the center to center of the orifice.

CHAPTER 4

RESULTS AND DISCUSSION

In this chapter, the discussion starts with the grid independence study followed by the CFD model validation. Finally, the hydrodynamics properties for nine different cases of models will be evaluated and discussed in detail for the following selected parameters of; Fluidization Velocity, Distributor Pressure Drop, Bed Expansion, and Jetting Velocity.

4.1 Grid Independence Study

The grid independence study is conducted to discover the optimum mesh size for the model which gives the most accurate results while consuming a moderate computational time. An independent grid is achieved when the numerical results do not change significantly with the increase in the mesh size. For this simulation, a grid independence study was carried out by plotting the air velocity across the BFB bed model and the values were compared for each mesh size used.

The comparison of the velocity results for different mesh sizes used in the grid independence study is depicted in Figure 4.1. The velocity plot of the same model was taken at the same position for four different meshing intervals of 0.005, 0.004, 0.003 and 0.002. Higher interval meshing value will give a smaller number of nodes compared to the lower interval value.

Figure 4.1 shows that there is no significant change in the velocity values using different mesh intervals. Hence it can be concluded that the grid is independent of the interval size and will not give any significant changes to the numerical results. In this study, 0.003 interval size has been chosen to be the mesh for all the models because it gave a minimum numerical error while consuming a decent computational time. The lower interval size is avoided because it may result in longer computational time without much improvement to the results.

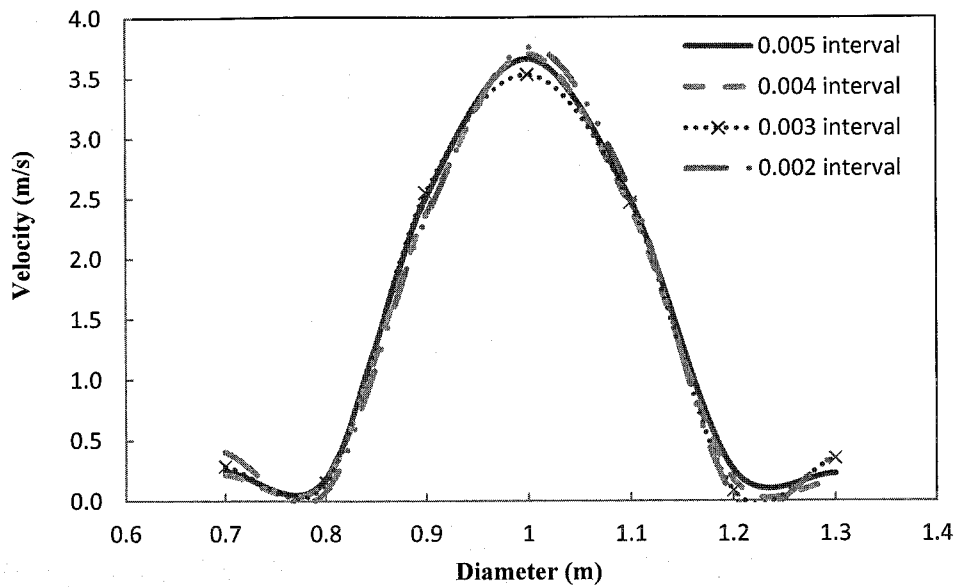


Figure 4.1: The velocity plot for different mesh interval used in the simulation

4.2 Hydrodynamics Model Validation

The CFD model was validated with the experimental results obtained by A. Busciglio *et al.* (2008). For the validation purpose, two hydrodynamics parameters from the experiment; the instantaneous bed height and the average bed height were used as parameters in comparing the simulation results to ensure the results are reliable and the model is representing the actual experiment.

Figure 4.2a shows the comparison between the instantaneous bed heights of the experiments by Busciglio *et al.* (2008) and the simulation from ANSYS Fluent 6.3, hereafter will be referred to as Fluent. For this case, the instantaneous bed height was validated for the air velocity ratio of $3.4 U_{mf}$. The measurements were taken for every 1 second time interval over 10 seconds of simulation time. From the figure it can be seen that the simulation is capable to produce similar trend in results as compared to the actual experimental data. Abnormalities can be seen at 7 s and 9 s which contradicted the trend in both cases, otherwise all others followed. On the whole the highest percentage of error observed between the experimental and simulation data varied by less than 5 percentage (%) at 7 s.

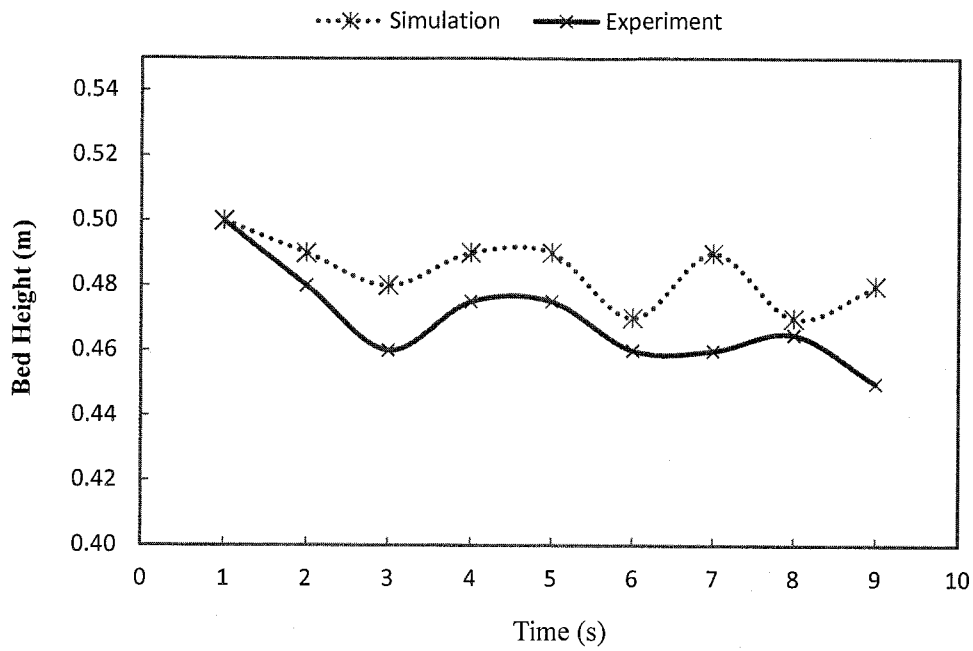


Figure 4.2a: Comparison of the Bed Height Simulation Results with the experimental data from Busciglio *et al.* (2008)

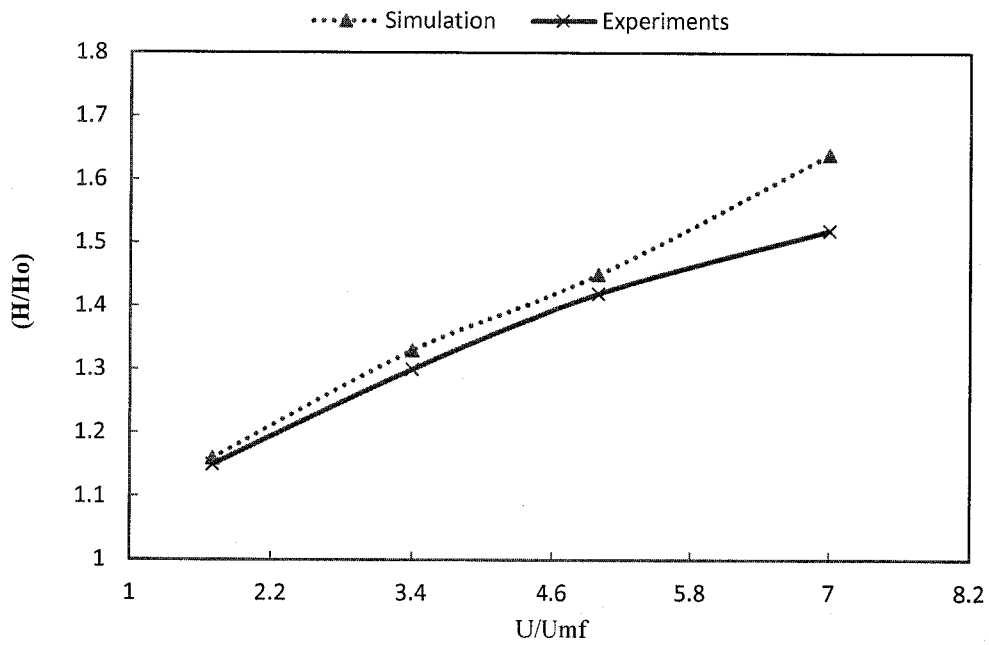


Figure 4.2b: Comparison of the Average Bed Height Simulation results with the experimental results from Busciglio *et al.* (2008)

The validation between the experiment and simulation was extended to the comparison of the average bed height ratio for four different superficial velocity ratios. The average bed height was calculated by taking the average bed height over 10 seconds of simulation time across the bed. The results from the simulation and experimental data are represented in Figure 4.2b. The average bed height ratio for the simulation and experiment show that the bed height increases with the increase of inlet velocity. It can be seen that both the simulation and experimental data show similar trend with an average difference of 0.03 for the values of U/U_{mf} below 5. For the values of U/U_{mf} higher than 5, the deviation increases further.

The validation model is capable to predict the hydrodynamics of the BFB based on Busciglio *et al.* (2008) model. From the comparison done it can be seen that the Fluent model predicted similar pattern but slightly higher value for instantaneous bed and mean expansion as compared to the experimental results. Therefore, we can further extend the simulation for different parameters.

The slightly higher value may be due to the limitation of the simulation model. In the simulation model (Fluent), the convection and diffusion fluctuation energy of solid particles were neglected thus implicating that the particles have higher energy compared to the actual process. Higher energy will make the particles move rapidly, creating smaller bubbles which tend to coalesce more frequently resulting in larger bubbles. Larger bubbles will give a larger bubble eruption thus making the instantaneous bed height to be higher.

4.3 Effect of Superficial Velocities to bubbling behavior on different orifice shapes

In the fluidization process, superficial velocity plays an important role in determining the fluidization regimes, whether the bed is operating in a packed bed, bubbling, or fast fluidization regimes. In the bubbling bed regime, superficial velocity has a direct effect on the bubbles' properties and characteristics where it influences the mixing and segregation of particles during the fluidization process.

In this sub-chapter, the effect of superficial velocities on different orifice shapes will be compared and the finding will be discussed for three different superficial velocity ratios, $1.33 U_{mf}$, $2.0 U_{mf}$, and $2.67 U_{mf}$ representing low, medium, and high velocity, respectively. In the simulation setup, the properties of air at a room temperature were used as the inlet gas properties and the bed particles properties used in the simulation consist of uni-diameter which fall in Geldard B group for all orifice shapes.

The effect of superficial velocity on the bubbling hydrodynamics will be represented in visual manner using a volume contour plot. The volume contour plots provide snapshots of images showing fractions of air, and sand particles during the fluidization process. The fraction scale on the left hand side is used to distinguish the fraction value for each phase. The red region on the plot represents the particulate phase while the blue region represents the air phase.

4.3.1 Cylindrical orifice

The contour plots in Figures 4.3.1a - 4.3.1c depict bubble formation for three inlet velocity ratios of $1.33 U_{mf}$, $2.00 U_{mf}$, and $2.67 U_{mf}$, respectively for the 13-cylindrical-orifice plate. It can be clearly seen from the contour plot that formed bubbles have different physical properties as well as hydrodynamic properties at different velocities. The most distinguished properties that can be observed from the plots are the size and frequency of the bubbles. At a low velocity, depicted by Figure 4.3.1a, the frequencies of the bubbles formed are less compared to a higher velocity, depicted by Figure 4.3.1c. The size of the bubbles increased with the inlet velocity, where small cloud-shaped bubbles can be observed at low inlet velocity, larger bubbles at $2.00 U_{mf}$, and even larger bubbles approaching slug size at $2.67 U_{mf}$. High frequency of bubbles formed at a higher velocity will coalesce with each other which

results in the formation of larger bubbles that travel upwards to the interphase region. When the bubbles rise from the bottom of the bed, the bubbles enhance the mixing process between the particulates.

Figures 4.3.1d to 4.3.1f depict the volume contour plot for 19-cylindrical-orifice plate. From the figures, we can see graphically that the size and frequency of bubbles are quite similar to 13-cylindrical-orifice plate case. However, if we examine closely by plotting the pressure drop and bed height (discussed further in sub-chapter 4.4 and 4.5), both of the cases did not share the same value, showing that the frequency and size of bubbles are different.

Figure 4.3.1g to Figure 4.3.1i show the contour for 39-cylindrical-orifice plate case. At a lower velocity of $1.33 U_{mf}$, no bubbles are visible throughout the simulation as shown in Figure 4.3.1g. This is due to the insufficient gas flow rate purging through the orifices. The inlet gas purging through the individual orifice is unable to sustain the force balance between buoyancy and the surface tension thus no bubbles are formed. The inlet gas only flow through the percolates of particles.

At $2.00 U_{mf}$, only a small frequency and diameters of bubbles can be observed as depicted in Figure 4.3.1h. The formations of the bubbles are quite unstable compared to 13-orifice and 19-orifice plate cases at the same inlet velocity. This however changes at higher inlet velocity of $2.67 U_{mf}$ where the frequency and the size of the bubbles increase. The instability in the formation of bubbles for the 39-orifice plate case can be related to the higher number of openings on the distributor plate. The large number of openings will reduce the pressure drop making the inlet gas lose its momentum thus affecting the uniform air distribution through each individual orifice.

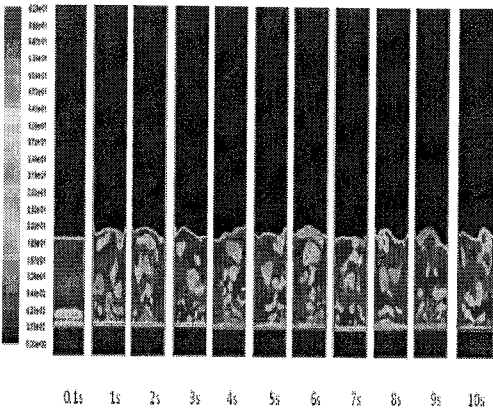


Figure 4.3.1a: Volume fraction contour at $1.33 U_{mf}$ for 13-cylindrical-orifice plate

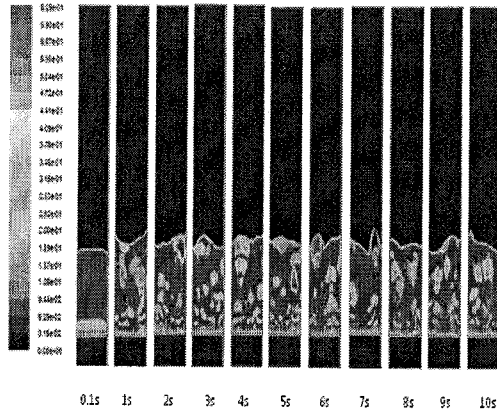


Figure 4.3.1b: Volume fraction contour at $2 U_{mf}$ for 13-cylindrical-orifice plate

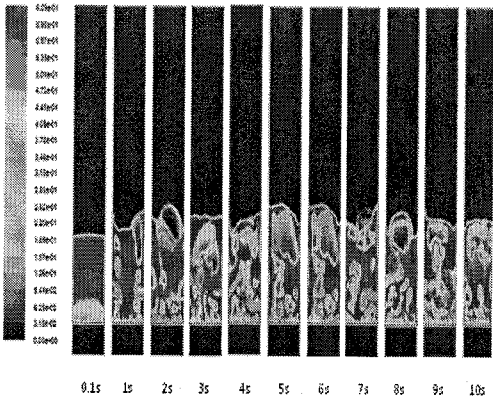


Figure 4.3.1c: Volume fraction contour at $2.67 U_{mf}$ for 13-cylindrical-orifice plate

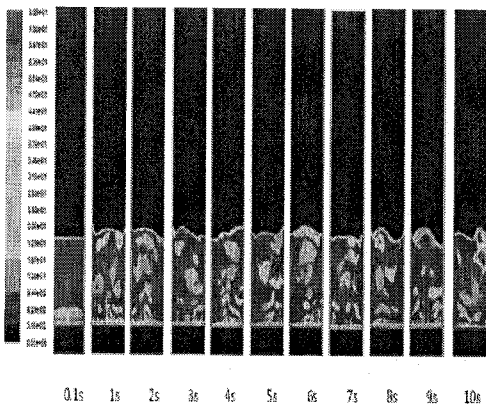


Figure 4.3.1d: Volume fraction contour at $1.33 U_{mf}$ for 19-cylindrical-orifice plate

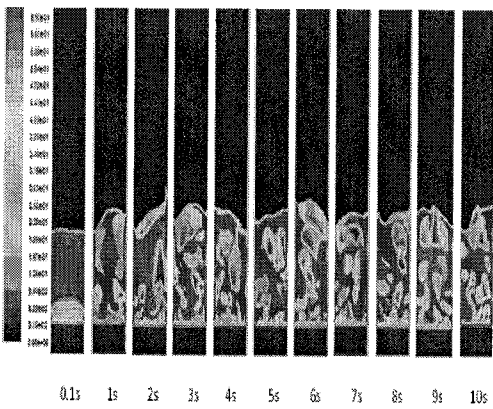


Figure 4.3.1e: Volume fraction contour at $2.00 U_{mf}$ for 19-cylindrical-orifice plate

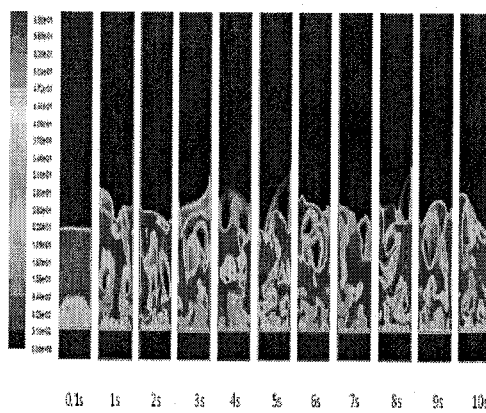


Figure 4.3.1f: Volume fraction contour at $2.67 U_{mf}$ for 19-cylindrical-orifice plate

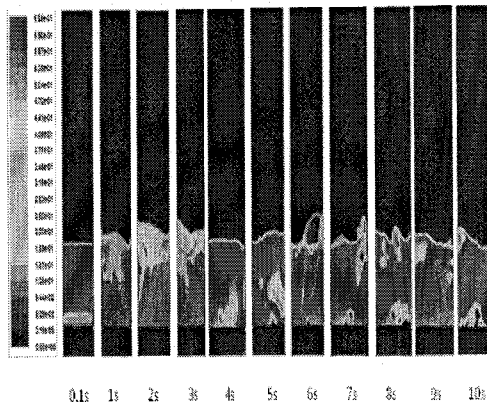


Figure 4.3.1g: Volume fraction contour at $1.33 U_{mf}$ for 39-cylindrical-orifice plate

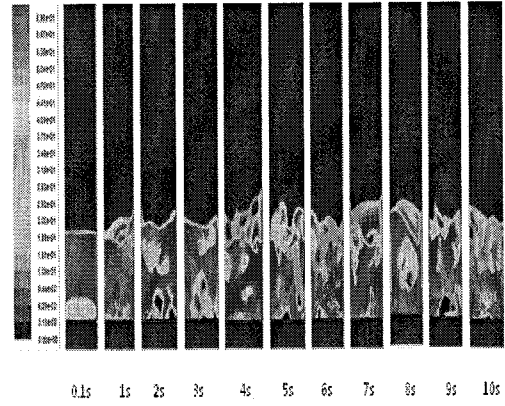


Figure 4.3.1h: Volume fraction contour at $2.00 U_{mf}$ for 39-cylindrical-orifice plate

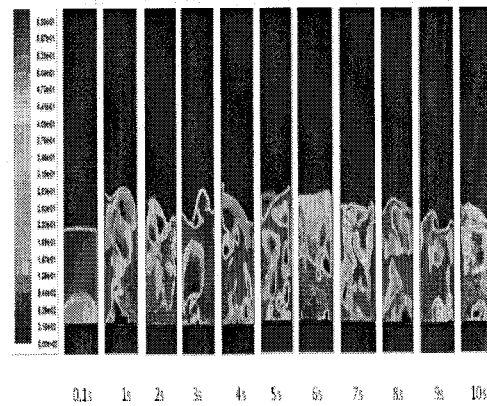


Figure 4.3.1i: Volume fraction contour at $2.67 U_{mf}$ for 39-cylindrical-orifice plate

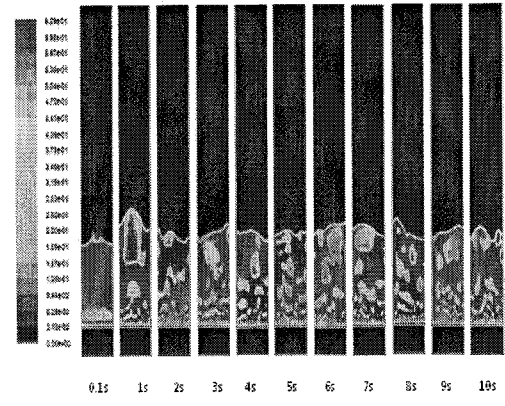


Figure 4.3.2a: Volume fraction contour at $1.33 U_{mf}$ for 13- diffuser -orifice plate

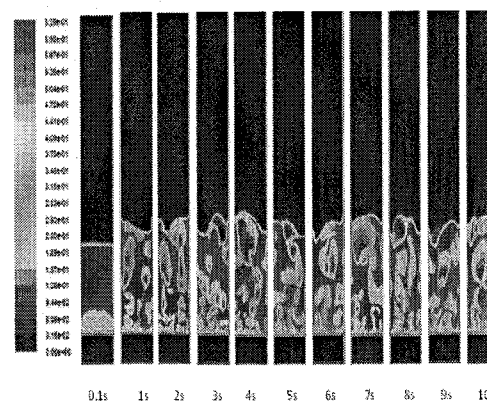


Figure 4.3.2b: Volume fraction contour at $2.00 U_{mf}$ for 13- diffuser nozzle-orifice

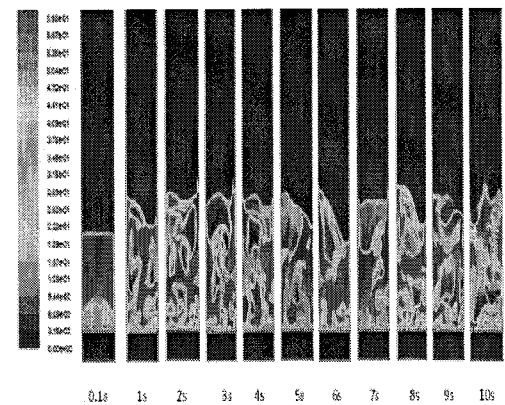


Figure 4.3.2c: Volume fraction contour at $2.67 U_{mf}$ for 13- diffuser -orifice plate

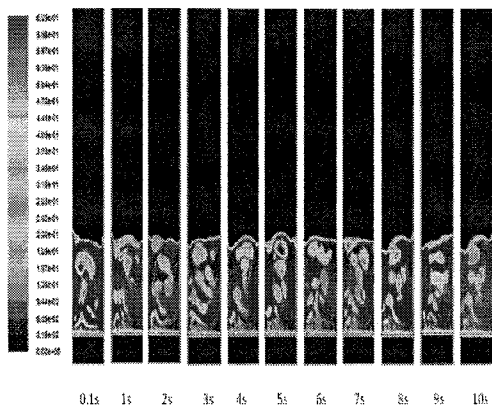


Figure 4.3.2d: Volume fraction contour at $1.33 U_{mf}$ for 19-diffuser-orifice plate

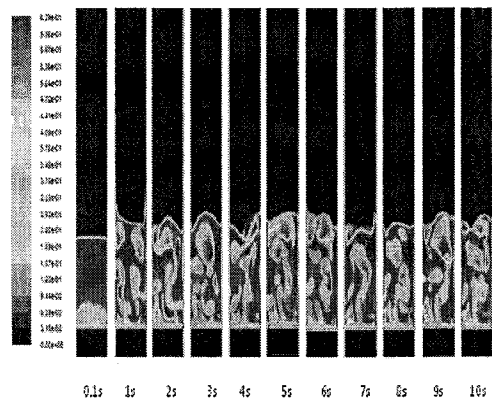


Figure 4.3.2e: Volume fraction contour at $2.00 U_{mf}$ for 19-diffuser-orifice plate

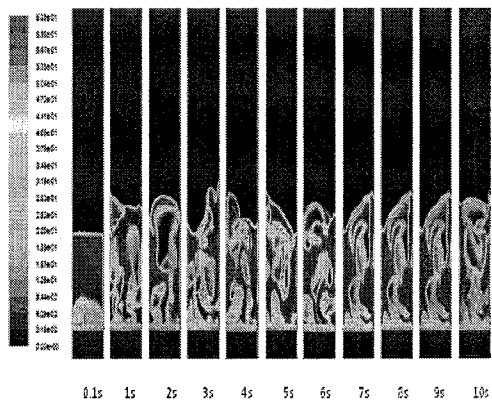


Figure 4.3.2f: Volume fraction contour at $2.67 U_{mf}$ for 19-diffuser-orifice plate

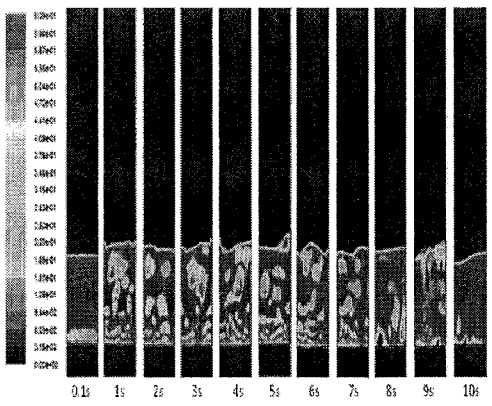


Figure 4.3.2g: Volume fraction contour at $1.33 U_{mf}$ for 39-diffuser-orifice plate

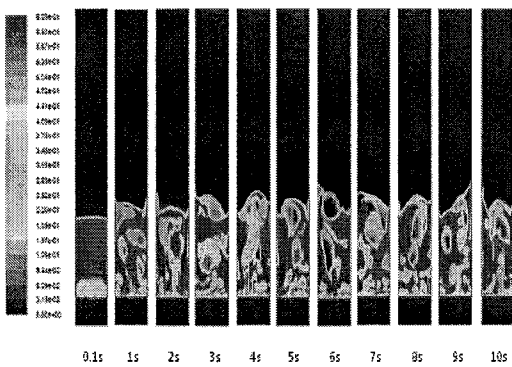


Figure 4.3.2h: Volume fraction contour at $2.00 U_{mf}$ for 39-diffuser-orifice plate

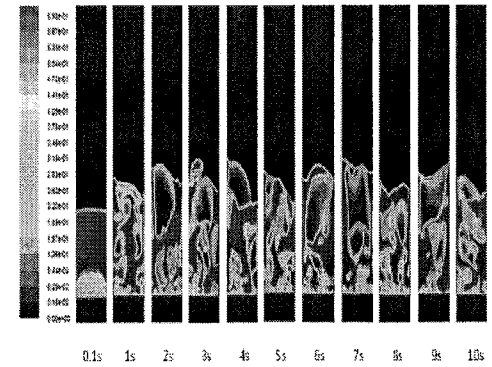


Figure 4.3.2i: Volume fraction contour at $2.67 U_{mf}$ for 39-diffuser-orifice plate

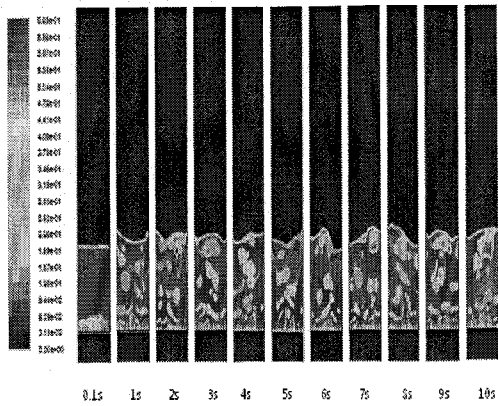


Figure 4.3.3a: Volume fraction contour at $1.33 U_{mf}$ for 13-nozzle-orifice plate

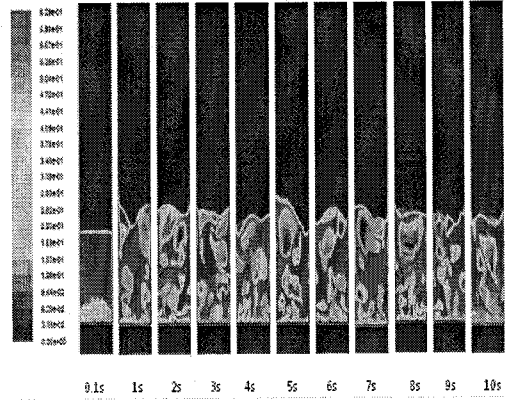


Figure 4.3.3b: Volume fraction contour at $2.00 U_{mf}$ for 13-nozzle-orifice plate

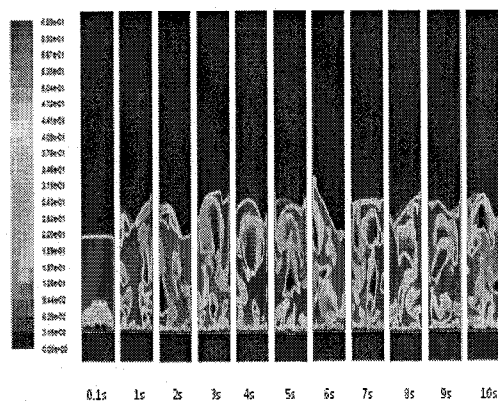


Figure 4.3.3c: Volume fraction contour at $2.67 U_{mf}$ for 13-nozzle-orifice plate

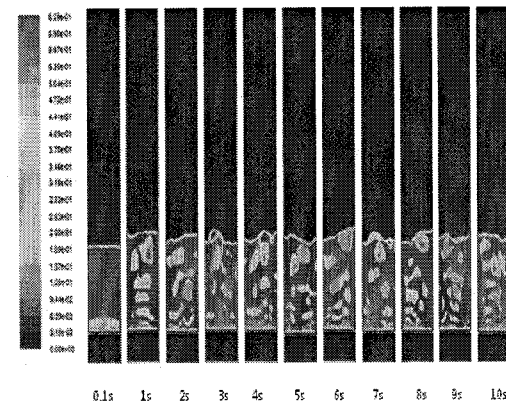


Figure 4.3.3d: Volume fraction contour at $1.33 U_{mf}$ for 19-nozzle-orifice plate

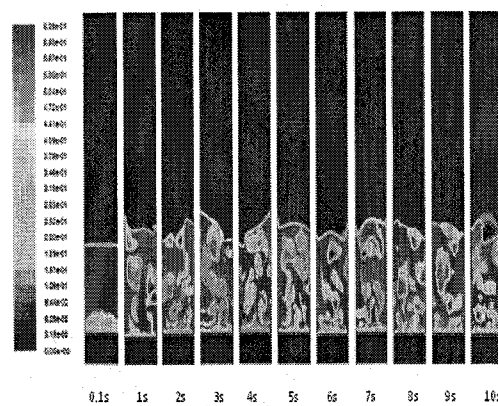


Figure 4.3.3e: Volume fraction contour at $2.00 U_{mf}$ for 19-nozzle-orifice plate

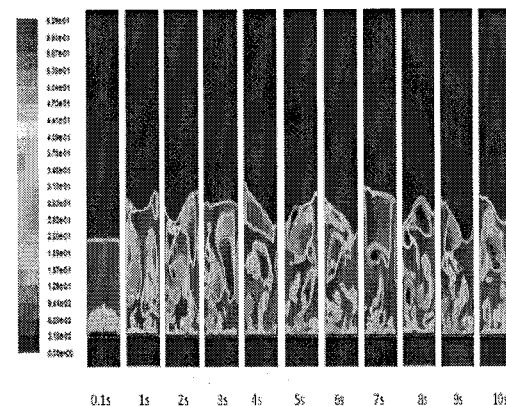


Figure 4.3.3f: Volume fraction contour at $2.67 U_{mf}$ for 19-nozzle-orifice plate

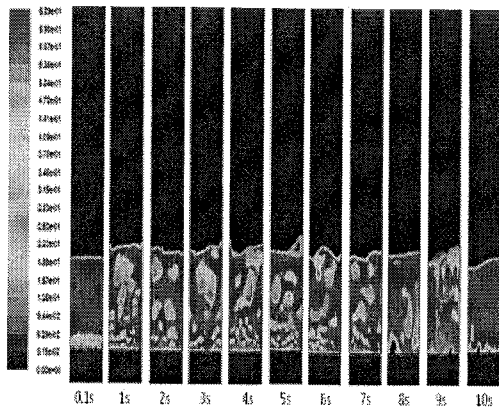


Figure 4.3.3g: Volume fraction contour at $1.33 U_{mf}$ for 39-nozzle-orifice plate

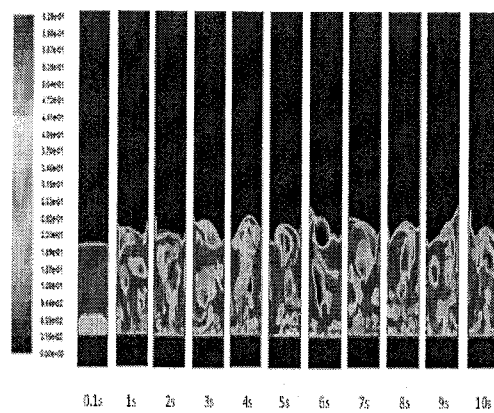


Figure 4.3.3h: Volume fraction contour at $2.00 U_{mf}$ for 39-nozzle-orifice plate

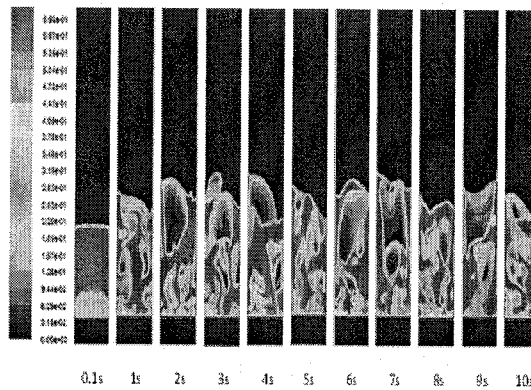


Figure 4.3.3i: Volume fraction contour at $2.67 U_{mf}$ for 39-nozzle-orifice plate

4.3.2 Diffuser Orifice

For the diffuser orifice, the volume contour plot for 13, 19, and 39-orifice plates are shown by Figures 4.3.2a to 4.3.2c, Figure 4.3.2d to 4.3.2f and Figure 4.3.2g to 4.3.2i, respectively. For the 13-orifice plate case, the same trend as the cylindrical orifice can be observed where small cloud-shaped bubbles are formed at low inlet velocity and the size and frequency of the bubbles will increase with increasing velocity. Although sharing the same trend, diffuser orifices are observed to provide higher frequency of bubbles compared to the cylindrical orifices at low inlet velocity.

As for the 19-orifice plate depicted by Figure 4.3.2d to 4.3.2f, the bubbles size are slightly larger compared to the 13-orifice plate case at low and medium velocities of $1.33 U_{mf}$ and $2.00 U_{mf}$. The bubbles are larger for 19-orifice plate case compared to 13-orifice plate case owing to rapid coalesce of bubbles near the distributor plate area for 19-orifice plate case as the distance between each individual orifice is much closer. At the higher superficial velocity of $2.67 U_{mf}$, the same trend of slug formation can be seen as the 13-orifice plate case.

For the 39-orifice plate, at lower velocity of $1.33 U_{mf}$, the bed produced smaller bubbles than the 13 and 19-orifice plate cases which can be observed in Figure 4.3.2g. However, at 8 second of simulation time, the bubbles are no longer visible rising from the plenum chamber of the bed. This is mainly due to the loss in momentum. At a higher superficial velocity of $2.00 U_{mf}$, the problem with the momentum loss is no longer present and the bubbles formation is found similar as in 19 numbers of orifices cases where both smaller and bigger bubbles can be observed from the bed. At $2.67 U_{mf}$, the bed expands rigorously compared to the other two cases.

4.3.3 Nozzle orifice

The contour plot for 13, 19, and 39-nozzle-orifice plates are shown by Figures 4.3.3a to 4.3.3c, Figure 4.3.3d to 4.3.3f and Figure 4.3.3g to 4.3.3i, respectively.

For the 13-orifice plate cases of $1.33 U_{mf}$, $2 U_{mf}$, and $2.67 U_{mf}$ inlet velocity, depicted by Figure 4.3.3a to 4.3.3c, similar contour plot and trend can be seen as the diffuser orifice case where the size of bubbles is directly proportional to the inlet velocity introduced through the bed.

The same observation can also be implied to 19 and 39 number of orifices cases. Figure 4.3.3g depicts the same observation as Figure 4.3.2g where no bubbles were visible after 8 second of simulation time due to loss in air momentum. Although the size and the frequency of the bubbles produced for this case are similar to the other cases before, the traveling paths and coalescing patterns however is not entirely identical.

4.4 Effect of different Orifice shapes on the Distributor Pressure Drop

Apart from the superficial velocity, distributor pressure drop also has a significant effect upon the fluidization quality. Generally, distributor plates with a higher pressure drop are favorable as they can provide more uniform air distribution which results in a better fluidization quality and superior gas-solid contacts.

In this study, in order to measure the pressure drop across the distributor plate for all three orifice shapes, two points located 0.01 m above and below the distributor plates were used as the reference points. The air pressure will be measured for both points, and the difference between them will be taken as the average pressure drop across the distributor plate.

4.4.1 Distributor Pressure Drop for Different number of orifices

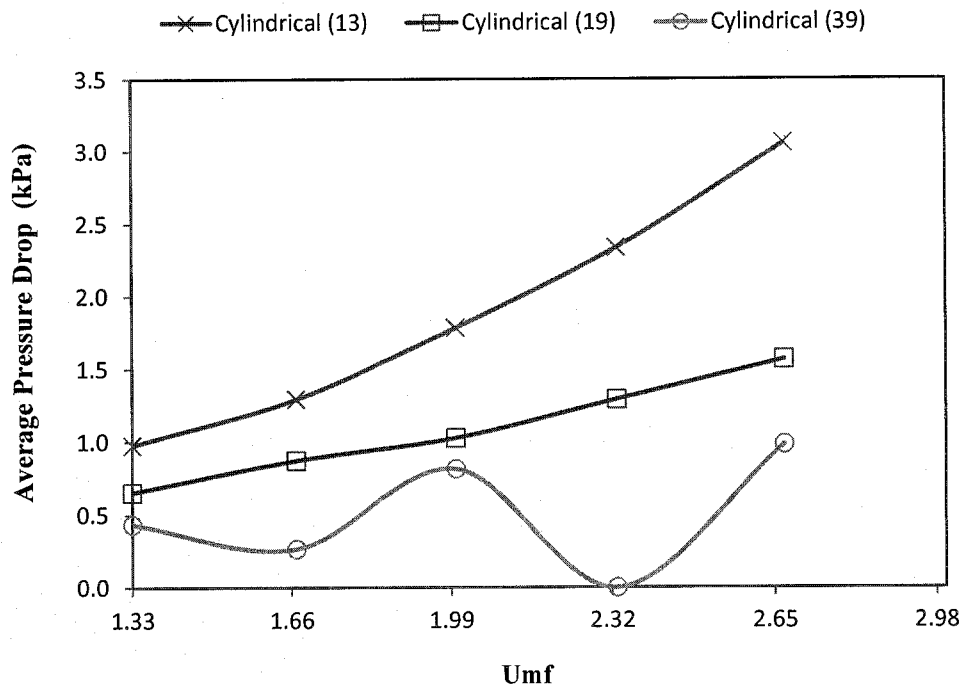
Figures 4.4a to 4.4c depict the comparison of the average distributor pressure drop for 13, 19, and 39-orifice plates for each orifice type, Cylindrical, Nozzle, and Diffuser, respectively taken at five different superficial velocities.

The average distributor pressure drop plot for the cylindrical orifice is shown in Figure 4.4a. It can be seen that there exists a proportional relationship between the air inlet velocities and the distributor pressure drop for the 13 and 19-orifice plates. The same cannot be said for the 39-orifice plate. Although they (13 and 19-orifice plates) share the same trend in pressure drop value, 13-orifice plate exhibits a much higher pressure drop than the 19-orifice plate. The difference becomes more significant at a higher superficial velocity where at $2.67 U_{mf}$, the average pressure drop depicted by the 13-orifice plate increases by 2.0 kPa as compared to that at $1.33 U_{mf}$. For the same range of velocity, for the 19-orifice plate, the pressure drop increase is much lower (0.24 kPa). A different trend is observed for the 39-orifice plate. It peaks initially at $2.00 U_{mf}$, thereafter drops to almost zero at $2.33 U_{mf}$ and starts to peak again sharply after $2.33 U_{mf}$ following similar trend to that of 13 and 19-orifice plates.

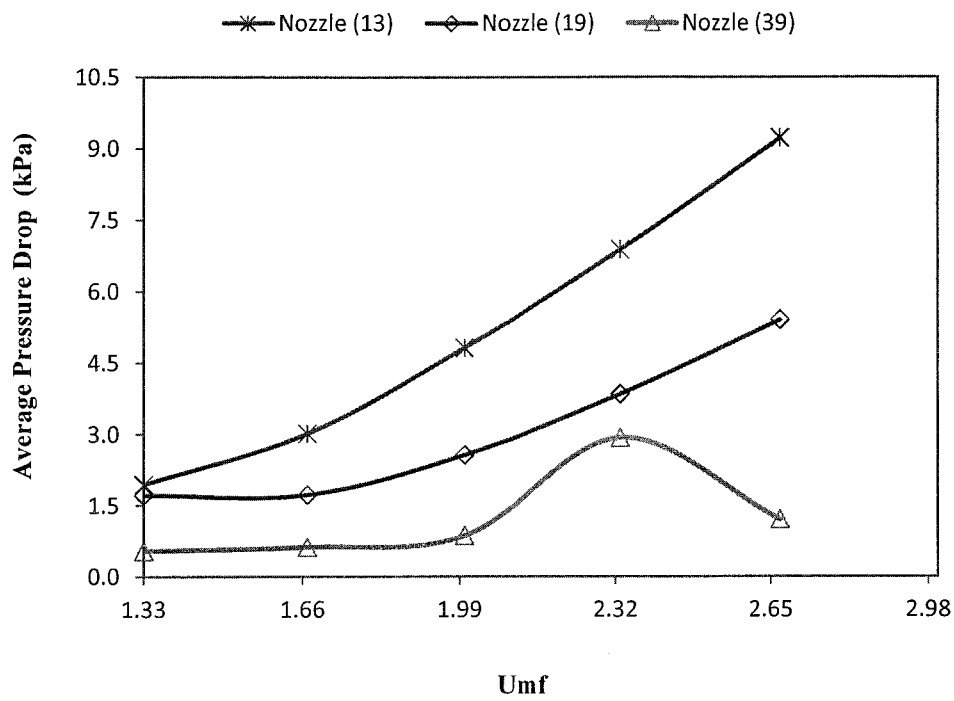
For the nozzle orifice, a similar trend as the cylindrical-shaped orifice can be observed from Figure 4.4b. Both the 13 and 19-orifice plates have the same pressure drop at $1.33 U_{mf}$, but the pressure drop for 13-orifice plate increases at a much faster rate than 19-orifice plate. The increase in pressure drop from 1.33 to $2.67 U_{mf}$ for 13 and 19

nozzle orifices is 8.5 and 3.7 kPa, respectively. In the case of 39-nozzle-orifice plates, the average pressure drop increases slightly with the increase of superficial velocity from 1.33 to 2.00 U_{mf} and depicts a sudden pressure drop increase at 2.33 U_{mf} before going down again at 2.67 U_{mf} .

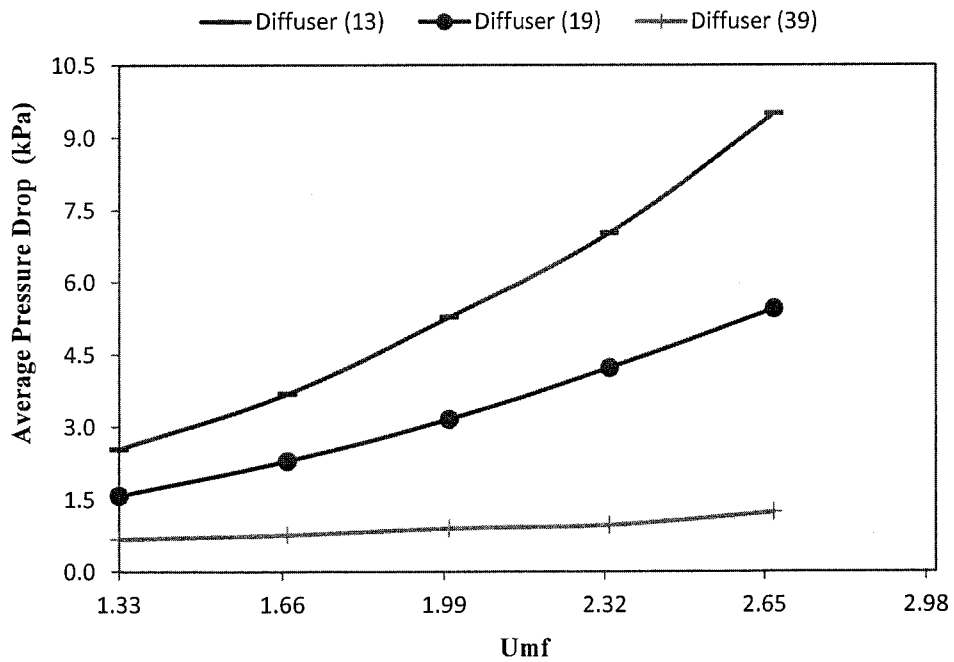
The comparison is also made for the diffuser orifice depicted by Figure 4.4c. A similar proportional trend where the average pressure drop increases with the increase of U_{mf} can be observed for both 13 and 19-diffuser-orifice plates as the cylindrical and nozzle shaped orifices. The increase in average pressure drop from 1.33 to 2.67 U_{mf} for 13 and 19-diffuser-orifice plates is 6.9 and 3.9 kPa, respectively. For the 39-orifice plate, a slight increase in pressure drop of 0.2 kPa is observed and it shared the same trend as the 13 and 19-orifice plates, which is directly proportional with the superficial velocity.



Figures 4.4a: Average distributor pressure drop at different velocities ratios for 13, 19, and 39 number of cylindrical orifices



Figures 4.4b: Average distributor pressure drop at different velocities ratios for 13, 19, and 39 number of Nozzle orifices



Figures 4.4c: Average distributor pressure drop at different velocities ratios for 13, 19, and 39 number of Diffuser orifices

In general, the distributor pressure drop has a proportional relation with the superficial velocity for 13 and 19-orifice plates for all three orifice shapes. The proportional relation between these parameters was reported by Sh. Saberi *et al.* (1995) in their study where the pressure drop increase with the increase of superficial velocity. From the figures, a similar observation as reported by Saxena *et al.* (1979) can be observed where the highest pressure drop was shown by the lowest opening ratio plate, 13-orifices plate, followed by 19-orifices plate and 39-orifices plate.

4.4.2 Distributor Pressure Drop for Different Orifice Shapes

In summary when comparing the 3 types of orifice for 13-orifices plate for pressure drop changes between 1.33 to 2.67 U_{mf} velocity range, it can be seen that the diffuser type exhibits the largest pressure drop of 9.4 kPa followed by nozzle (9.0 kPa) and cylindrical type (3.06 kPa) at 2.67 U_{mf} . Both diffuser and nozzle type orifices show the highest increase with the increase of superficial velocity compared to cylindrical type orifice as shown in Figure 4.4d.

For the 19-orifice plate plot depicted by Figure 4.4e with the same range of U_{mf} as above, the pressure drop shows similar trends but the average pressure drop values are 2 times lower compared to 13-orifice plate case. Diffuser and nozzle orifice plates share the same value of 1.7 kPa and 5.5 kPa at 1.33 U_{mf} and 2.67 U_{mf} , respectively. The cylindrical orifice shows an increment of 0.9 kPa over the superficial velocities range and still provides the lowest pressure drop compared to the other two.

In the case of 39 orifices shown in Figure 4.4f, diffuser orifice provides an increase of 0.8 kPa pressure drop from 1.33 U_{mf} to 2.67 U_{mf} . For the cylindrical orifice, instead of having a direct proportional trend as before, the average pressure drop that can be observed fluctuates through all the superficial velocity range. As for the nozzle, it shows a stable increment in pressure drop and provides a sudden increase from 0.6 kPa at 2.00 U_{mf} to 2.9 kPa at 2.33 U_{mf} , at a higher velocity of 2.67 U_{mf} , the pressure drop value dropped back to 1.2 kPa.

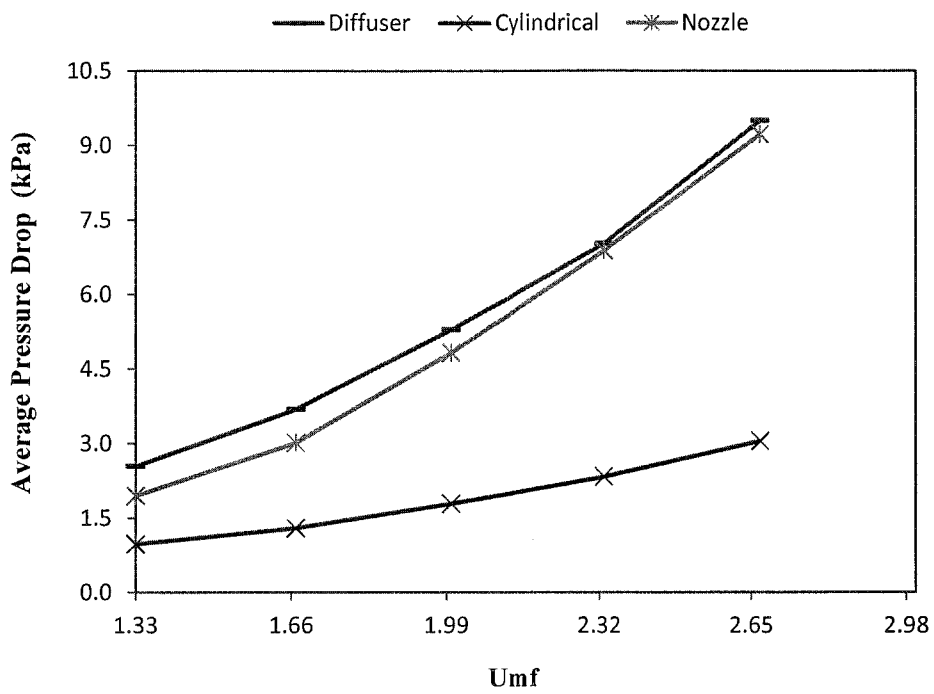


Figure 4.4d: Average distributor pressure drop taken at different velocities ratios for 13 numbers of orifices cases

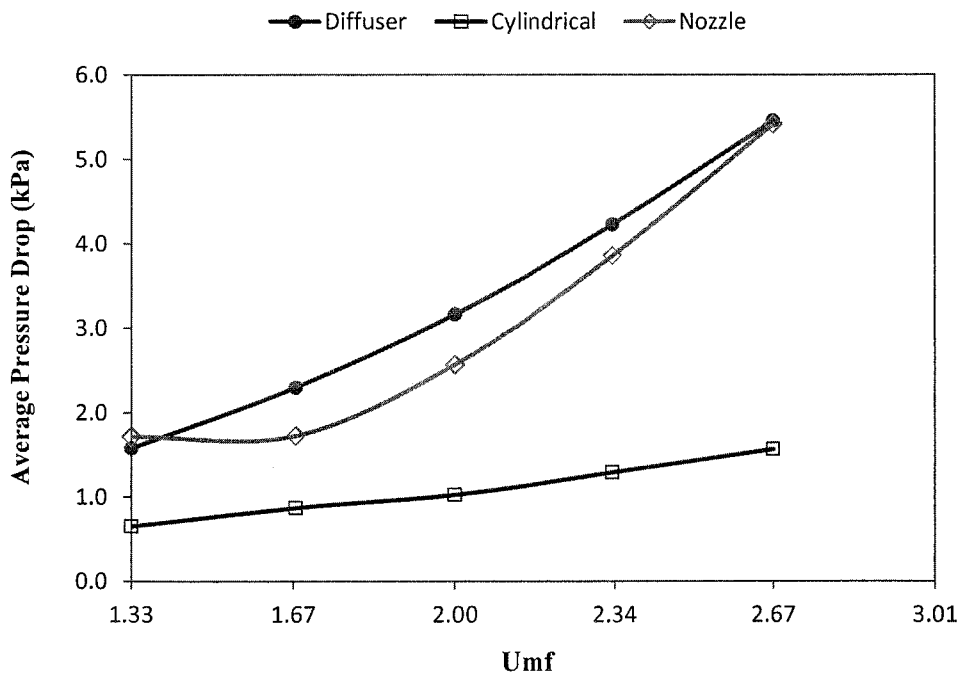


Figure 4.4e: Average distributor pressure drop taken at different velocities ratios for 19 numbers of orifices cases

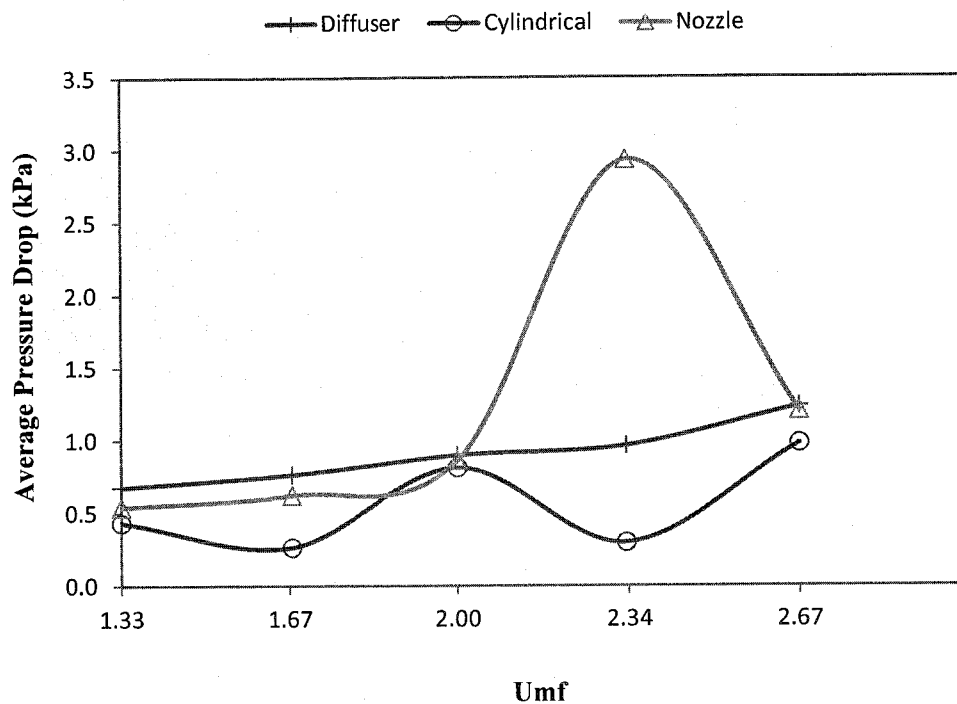


Figure 4.4f: Average distributor pressure drop taken at different velocities ratios for 39 numbers of orifices cases

A general trend that can be observed from Figure 4.4d-4.4f is that diffuser orifices have the highest average pressure drop for almost all the superficial velocity used in the simulation, followed by nozzle orifices, and then cylindrical orifices for 13 and 19-orifice plate cases. For the 39-orifice plate case, there is some abnormality found with the stated trend. It can also be observed that both diffuser and nozzle tend to share the same average pressure drop value at higher velocity ($2.67 U_{mf}$) and at lower velocities, diffuser provides slightly larger pressure drop value.

For the 13 and 19-orifice plate cases, the proportionality trend between the pressure drop and the superficial velocity can be explained by the presence of backpressure below the distributor plate. Higher superficial velocity means higher air flow purging in to the bed resulting in enormous backpressure created below the distributor plate, hence providing a higher pressure drop across the plate.

The fluctuation in the distributor pressure for 39 cylindrical orifice case happened because of the momentum loss of the air phase due to low pressure drop. The bubbles that were produced at earlier stage collapse instantly giving a non-uniform

pattern throughout the simulation. The fluctuation is dampening for nozzle and diffuser orifice because the orifice geometry having a smaller opening area above and below the plate respectively which provides them an advantage on retaining the momentum.

The simulations for all three orifices show that the highest pressure drop can be obtained by using a distributor plate with the least number of orifices. The low opening ratio will limit the air capability to purge into the bed region thus creating enormous backpressure below the plate while the plate with a high opening ratio will reduce the air resistivity from purging in.

4.5 Effect of Different superficial Velocity on Bed Expansion

Observing Bed expansion of the fluidized bed can provide information on the bubbles dynamic and the uniformity of the fluidization. In this sub-chapter, the average bed expansions for all three types of orifices (diffuser, nozzle and cylindrical) each with different numbers of orifices (13, 19, and 39) were plotted at different superficial velocity for 10 seconds of simulation time on 5 different inlet velocity ratios (U_{mf}). In each of the case the average bed size expansion ratio was measured and calculated for different velocity ratio and presented from Figure 4.5a – 4.5f. In Figure 4.5a–4.5c, individual orifice type was simulated and analyzed for the effect of orifice number, and then from Figure 4.5d–4.5f, the orifice number was fixed and was compared to the changes in orifice type. This was incorporated to have a better understanding and for simplicity for observation and explanations.

Figure 4.5a depicts the average bed expansion ratio for a diffuser orifice shape for 13, 19 and 39-orifice plates. 13-orifice plate gives the highest bed expansion followed by 19-orifice plate and the least expansion is shown by 39-orifice plate for all the various range of U_{mf} . From the same figure it can be seen that that higher the U_{mf} value the higher the bed expansion.

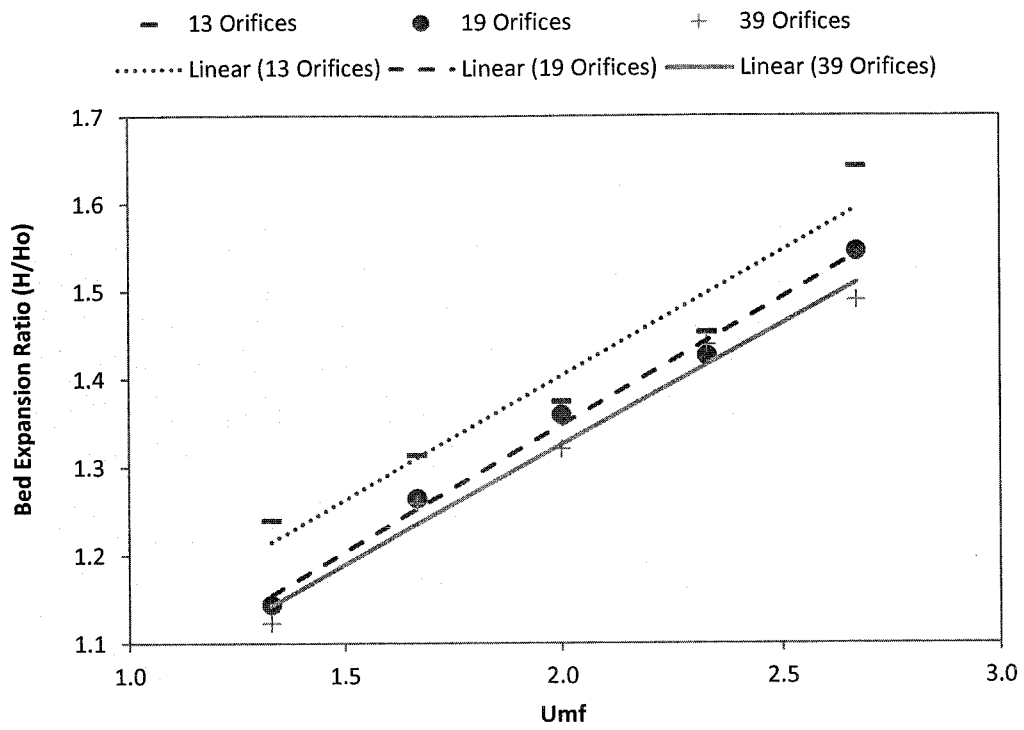


Figure 4.5a: Average Bed expansion ratio at different velocity ratio for Diffuser orifice shape

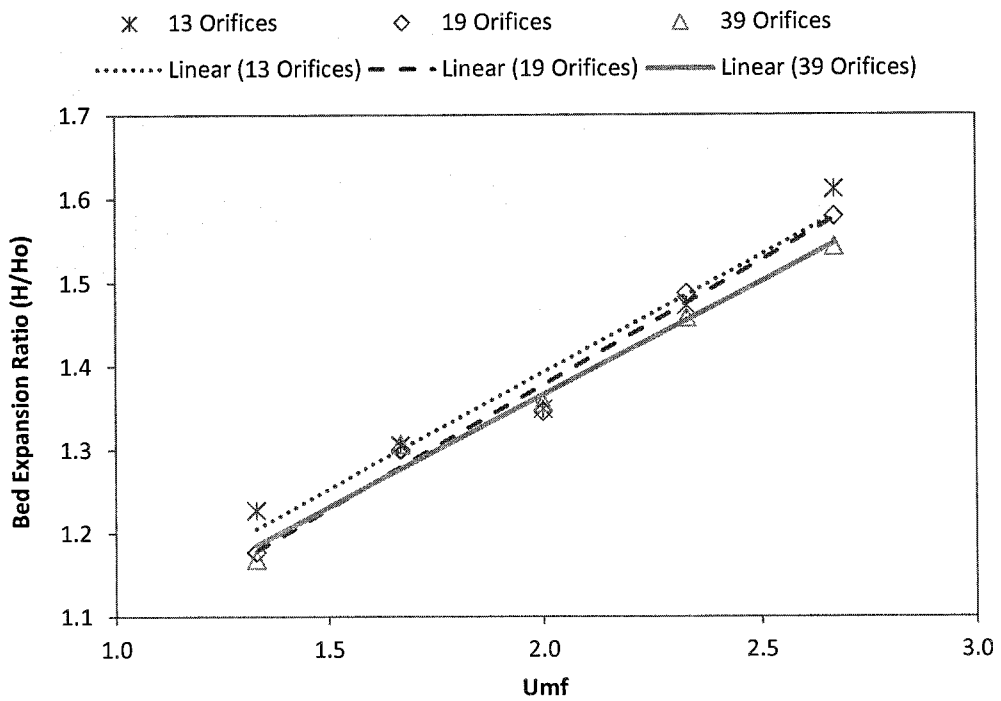


Figure 4.5b: Average Bed expansion ratio at different velocity ratio for Nozzle orifice shape

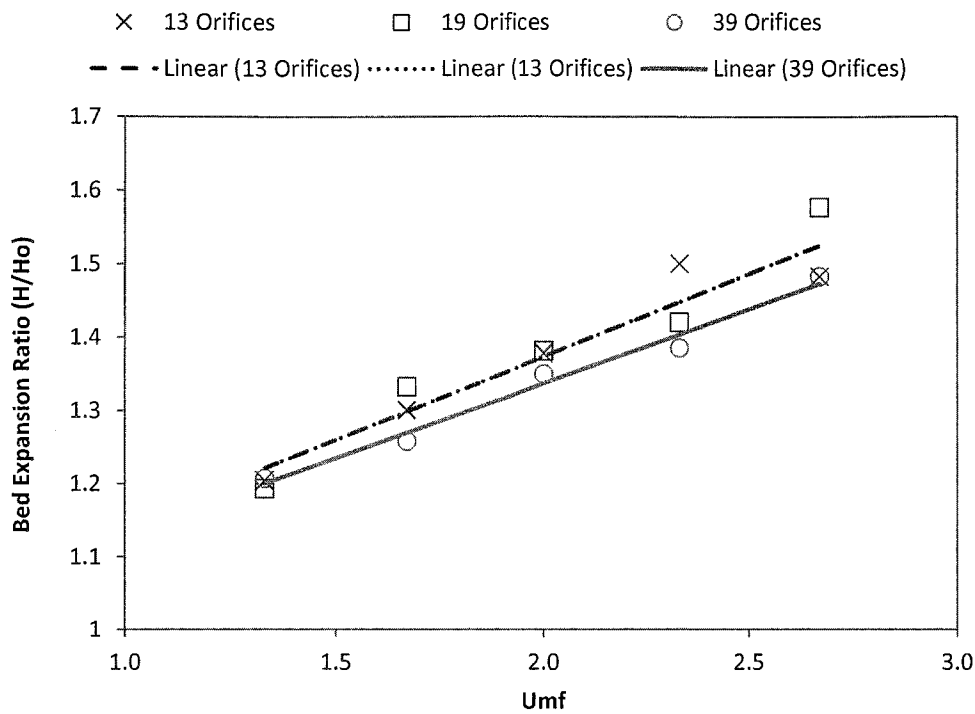


Figure 4.5c: Average Bed expansion ratio at different velocity ratio for cylindrical orifice shape

Figure 4.5b and 4.5c show the average bed expansion for nozzle and cylindrical orifices, respectively. Both plots provide the same trend where the expansions of the bed increase with increase in superficial velocity, but unlike diffuser type where all 3 number of orifices (13,19 and 39) can be distinguished, for the nozzle type, 19 and 39 orifices results are similar initially, but only differ at higher U_{mf} . The cylindrical orifice on the other hand, shows similar results for the 13 and 19 orifice for the whole of the measured U_{mf} . The same observations were reported by Sayyed Hossein Hosseini *et al.* (2010) and Poulouse M. M. *et al.* (2006) in their study. From this observation it can be said that both the cylindrical and nozzle orifices do not show much difference between the changes in number of orifice unlike diffuser type.

Increasing the superficial velocity will increase the air flow through the orifices thus producing a large number of small bubbles. These bubbles will coalesce with each other and as a result, bigger bubbles are produced while traveling up into the interphase region and collapse. The bubbles explosion will send the bed medium further up thus explaining the high bed expansion.

Apart from the superficial velocity, orifices size also plays an important part. Small opening orifice tends to have a higher bed expansion compared to the orifice with bigger opening. This is because distribution plate with a small opening tends to produce bigger bubbles through coalescence compared to the distribution plate with a large opening at the same superficial velocity. The explosion of bigger bubbles in the bed medium tends to send bed material to higher levels further up the chamber resulting in bed expansion.

A comparison for the average bed expansion for different orifices with the same orifices number are presented in Figure 4.5d to 4.5f for 13, 19, and 39 number of orifices, respectively. Figure 4.5d depicts that all 3 types of orifice have similar bed expansion at low U_{mf} up to $1.8 U_{mf}$, but as the U_{mf} increases they start to separate with the increase in bed expansion as per diffuser > Nozzle > cylindrical.

In the case of the 19 numbers of orifices, the diffuser type has the lowest bed expansion throughout the whole measured U_{mf} , but it is different for nozzle and cylindrical orifice. In the case of cylindrical orifice, it starts at higher bed expansion at lower U_{mf} of 1.33 as compared to nozzle type orifice. After $2.0 U_{mf}$ and higher the nozzle bed expansion overtakes the cylindrical type orifice.

For the 39 number of orifices case shown in Figure 4.5f, diffuser-shaped orifice has the lowest average bed expansion for a velocity range between $1.33U_{mf}$ to $2.00U_{mf}$. This trend however only applies at the low velocity where it changed at a higher velocity range, from $2.33U_{mf}$ - $2.67U_{mf}$, the cylindrical orifice provides lower average bed expansion ratio compared to diffuser orifice. In the case of nozzle and cylindrical type the average bed expansion at low (up to 1.6) U_{mf} are similar but at higher U_{mf} , nozzle orifice average bed expansion is much higher than cylindrical orifice. In fact U_{mf} between 1.67 to 2.00 increases the bed expansion as per nozzle > cylindrical > diffuser, but after $2.2 U_{mf}$, the increase in bed expansion becomes as nozzle > diffuser > cylindrical.

In general, the bed expansion becomes more vigorous at a higher superficial velocity. The increase in the air flow at higher superficial velocities result in higher frequency of bubbles produced at the bottom of the bed. These high frequencies of

bubbles coalesce rapidly with each other and produce larger bubbles and even slugging.

The observations for the comparison showed that different orifice shapes provide unique bubbles diameter depending on the number of orifices; opening on the distributor plate. Cylindrical type orifice gives higher average bed height at low U_{mf} than either nozzle or diffuser orifice. At higher U_{mf} , nozzle orifice gives higher average bed height than either diffuser or cylindrical type orifice. As for the number of orifice, at low numbers both diffuser and nozzle shows similar bed expansion. At medium number of orifice, cylindrical and nozzle orifices show bed expansion. At high number of orifice and low U_{mf} , nozzle and cylindrical orifice show similar bed expansion, but with increase in U_{mf} , cylindrical and diffuser orifice show similar bed expansion.

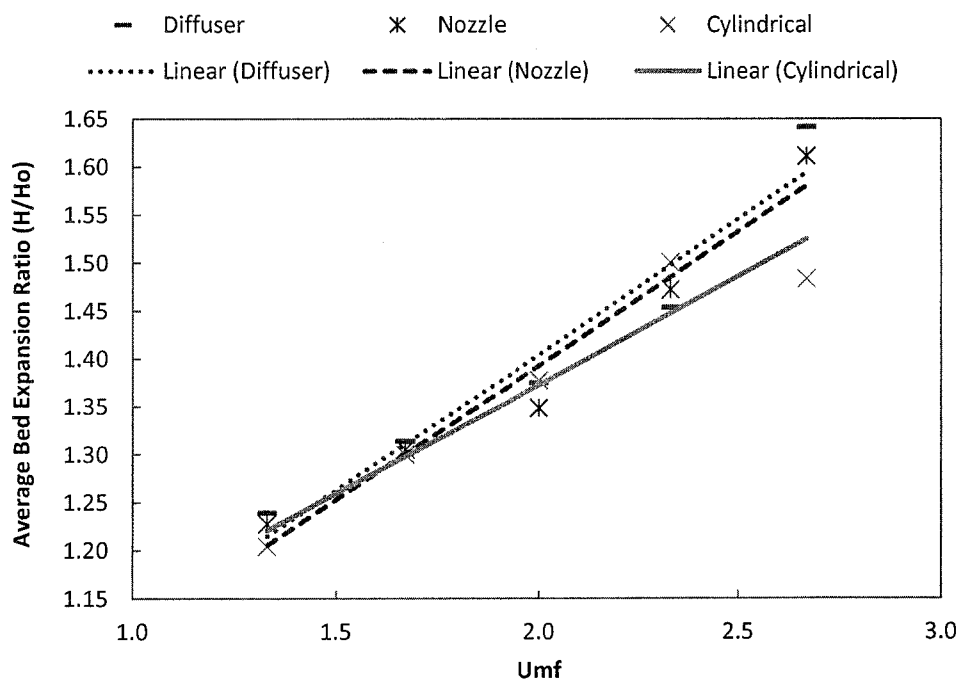


Figure 4.5d: Average Bed expansion ratio at different velocity ratio for 13-orifice plate

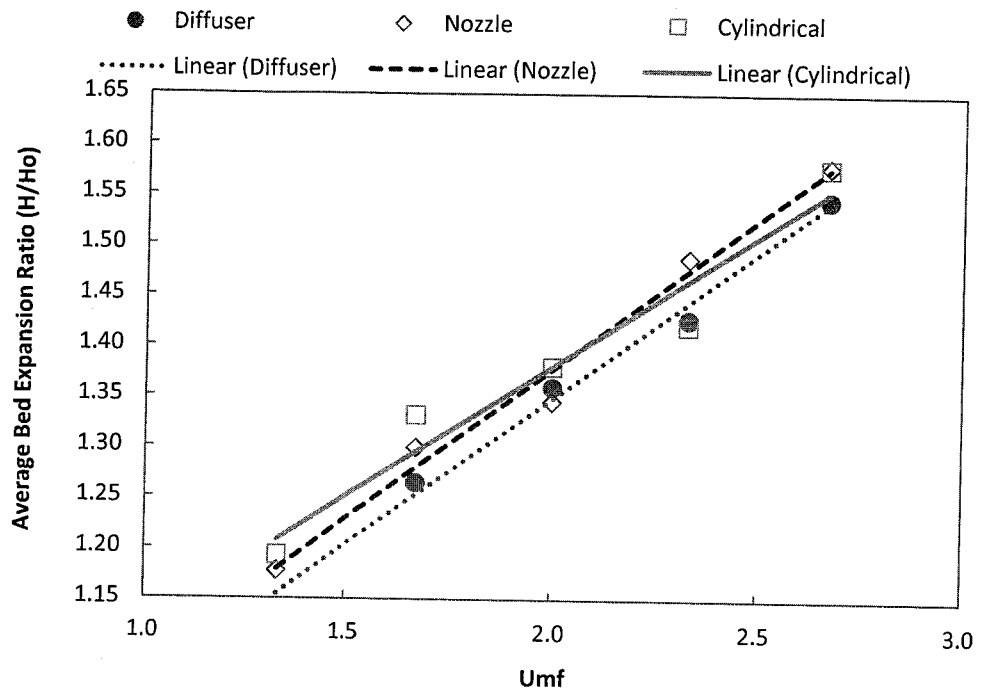


Figure 4.5e: Average Bed expansion ratio at different velocity ratio for 19-orifice plate

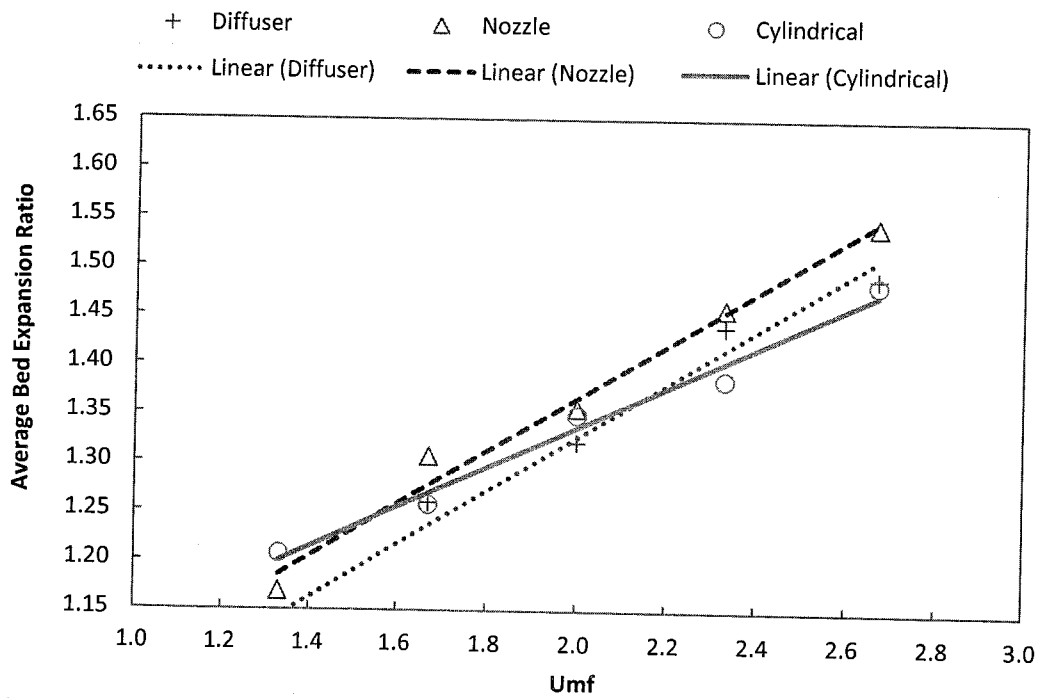


Figure 4.5f: Average Bed expansion ratio at different velocity ratio for 39-orifice plate

4.6 Effect of Different Jet Penetration Length on Different Orifice Shapes

The uniformity of the air flowing through the distributor plate with different orifice shapes can be interpreted from comparing the air velocity plot just above the distributor plate. Figures 4.6a to 4.6c depict an air velocity magnitude plot at different points throughout the bed width for 13, 19, and 39-orifice plates for all three orifices. The velocity magnitude readings were taken at a location, 0.01 m above the distributor plate at $1.67 U_{mf}$ and 2 seconds of simulation time for a reasonable fluidization simulation.

Figure 4.6a depicts the air velocities magnitude plot for the 13-orifice plates for diffuser, nozzle, and cylindrical orifices. A fluctuation of air velocity can be observed for all orifices types across the bed where the nozzle and diffuser orifices depict the smallest fluctuation and the cylindrical orifices provide the most unstable fluctuation trends. For 13-orifice plate case, diffuser has a slight advantage compared to other orifices shapes as it has higher gas penetration which can provide a better inter-particle mixing.

For the 19-orifice plate case, shown in Figure 4.6b, it can be seen that the nozzle orifice produces least fluctuation compared to diffuser and cylindrical orifices. Least fluctuation is a result of a uniform air flow through the plate. As for the 39-orifice plate case, nozzle and diffuser orifices give the same fluctuation trend while cylindrical orifices still provide the highest fluctuation.

In general, the number and orifices shapes have a significant effect on the bottom zone of a bubbling fluidized bed. A diffuser orifice provides a better fluidization for the orifices plate with the least number of orifices, 13-orifice plate compared to others. However, for the 19-orifice plate case, nozzle orifice shows a better and stable air velocity compared to diffuser orifice. For the highest orifices number on a plate, 39-orifice plate case, both nozzle and diffuser share a common trend where both can be observed to provide a stable gas velocity which results in a better fluidization in terms of inter-particle mixing.

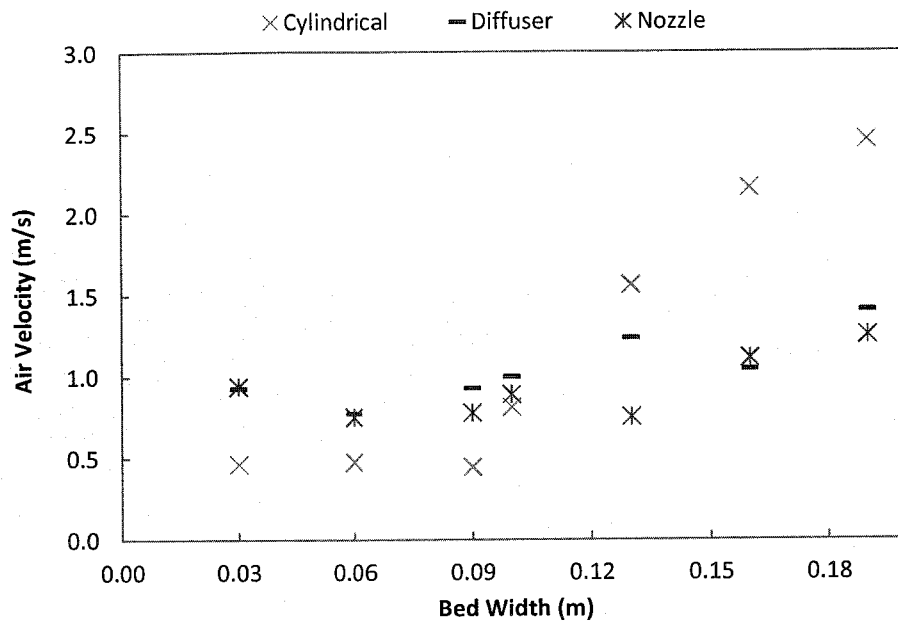


Figure 4.6a: Air Velocity plot through the bed width taken at 1.67 Umf, 0.01 m above the distributor plate for 13 numbers of Cylindrical, Diffuser and Nozzle orifices

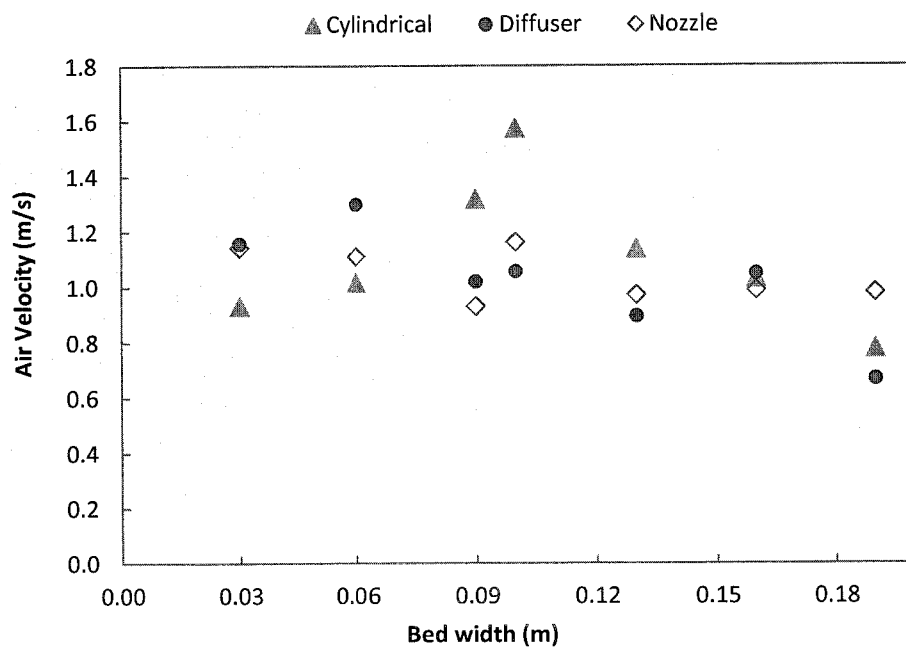


Figure 4.6b: Air Velocity plot through the bed width taken at 1.67 Umf, 0.01 m above the distributor plate for 19 numbers of Cylindrical, Diffuser and Nozzle orifices

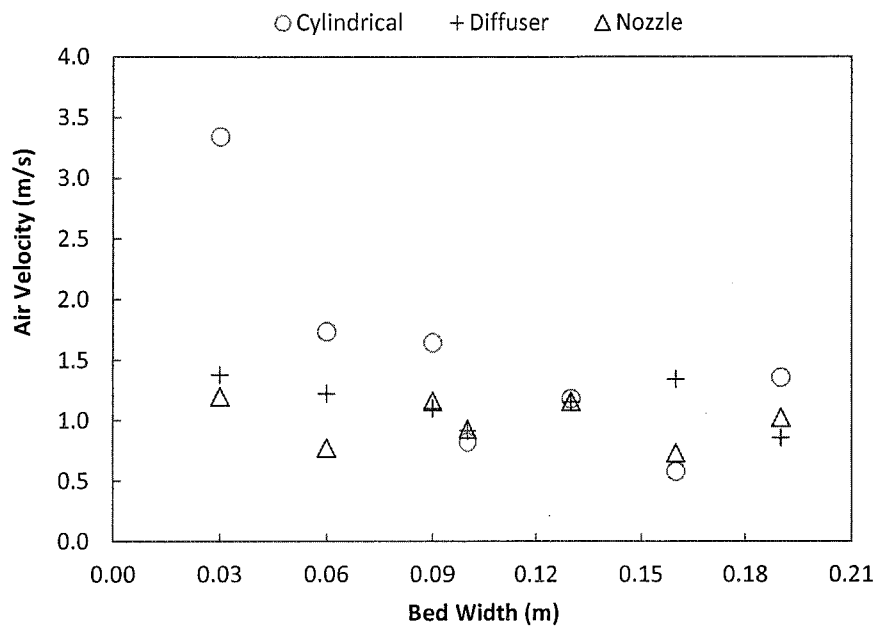


Figure 4.6c: Air Velocity plot through the bed width taken at $1.67 U_{mf}$, 0.01 m above the distributor plate for 39 numbers of Cylindrical, Diffuser and Nozzle orifice

CHAPTER 5

CONCLUSION AND RECOMMENDATIONS

5.1 Conclusion

The effect of distributor plate on the fluidization hydrodynamics has been studied in this work numerically using the ANSYS Fluent software. The total numbers of nine (9) models have been successfully developed for different orifice shapes and numbers of orifices. The objective of the study is to investigate the most suitable orifice shape to improve the fluidization stability.

Based on the observation from the simulation study, different orifice shape and different plate opening will have different pressure drop value thus have a significant impact to the hydrodynamic of fluidization.

Effect of different number of orifices for cylindrical, nozzle, and diffuser shape were compared on the pressure drop across the plate. All of the orifices provide the same general observation. Plate with the lowest opening will have highest pressure drop thus can provide the most stable fluidization throughout the process while plate with the highest opening ratio or highest number of orifices tend to provide a poor fluidization as the pressure builds up below the plate is low thus could not constantly exceeded pressure on the bed. A comparison is then plot for different number for 13, 19, and 39 opening. From the observation, diffuser shape provides the highest pressure drop compared to nozzle and cylindrical shape.

On the shape of the orifice, nozzle shape provide the most stable bed expansion for 13 and 19 orifices plate cases compared to the cylindrical and diffuser orifice. The stable fluctuation of the bed expansion mirror the bubble formation, showing smaller bubbles were formed in the bed thus provide a better mixing and heat distribution. It is concludes that even the highest pressure drop is favourable to provide a stable fluctuation and bed expansion; it is not entirely perfect as the effect of the orifices also affect the fluctuation.

5.2 Recommendation

In the present study, the openings of the distributor are limited by three (3) numbers only with a uniform distance between the orifices and the same shape of plenum chamber. A further study can be done by varying the orifice distance to get the most stable fluidization through the bed as well as varying plenum chamber design.

Instead of using only one Geldard particle group, different Geldard group can be used as a variable parameter, to make sure which distributor type provide the most efficient air distribution through the bed for each Geldard group.

REFERENCES

1. A.Samuelberg and B. H. Hjertager, "An Experimental and Numerical study of flow patterns in a circulating fluidized bed reactor," *Int. J. Multiphase Flow*, Vol. 22, No. 3, pp. 575-591, 1996.
2. Alberto Di Renzo, Francesco Paolo Di Maio, "Homogeneous and bubbling fluidization regimes in DEM-CFD simulations: Hydrodynamic stability of gas and liquid fluidized beds," *Chemical Engineering Science*, Vol. 62, Issues 1-2, pp. 116-130 January 2007.
3. ANSYS, Inc FLUENT 6.3 User Guide, Revised January 30, 2009
4. Agarwal J. C., Davis W. L., and King D. T., "Fluidized-bed Coal dryer," *Chemical Engineering Progress*, Vol. 58, No.11, pp. 85-90, 1962.
5. Athirah Mohd Tamidi, Ku Zilati Ku Shaari, "Effect of Steam Inlet Velocity and Solid Initial Bed Height to the Hydrodynamics of Fluidized Bed Gasifier," *Journal of Applied Sciences*, Vol 10, pg 3257-3263, 2010.
6. Athirah Mohd Tamidi, Ku Zilati Ku Shaari, Suzana Yusup, Lau Kok Keong, "Model Development for Hydrodynamic Study of Fluidized Bed Gasifier for Biomass Gasification," *Journal of Applied Sciences*, Vol 11, pp 2334-2339, 2011.
7. Antonio Busciglio, Giuseppa Vella, Giorgio Micela, Lucio Rizzoti, "Analysis of the Bubbling Behavior of 2D gas solid fluidized bed. Part II Comparison between experiments and numerical simulation via Digital Image Analysis Technique," *Chemical Engineering Journal*, Vol. 148, pp.145-163, 2009.

8. B.G.M. van Wachem, , J.C. Schoutena, R. Krishnab, C.M. van den Bleeka, "Eulerian simulations of bubbling behaviour in gas-solid fluidised beds," *Computers & Chemical Engineering*, Vol. 22, Supplement 1, pp. S299–S306, 15 March 1998.
9. B.H. Xu, A.B. Yu. "Numerical simulation of the gas-solid flow in a fluidized bed by combining discrete particle method with computational fluid dynamics," *Chemical Engineering Science*, Vol. 52, No. 16, pp. 2785 2809, 1997.
10. Botterill J. S. M., Teoman Y. and Yuregir K. R., "The effect of Operating Temperature on the velocity of minimum fluidization, bed voidage, and general behaviour," *Powder Technology*, Vol. 31, pp101-110, 1982.
11. C.C Pain, S. Mansoorzadeh, C.R.E. de Oliveira "A study of bubbling and slugging Fluidised beds using the two fluid granular temperature model," *International Journal of Multiphase Flow*, Vol. 27, pp. 527-551, 2001.
12. C. J. Chen, R. Bernatz, K. D. Carlson, and Wanlai Lin, "Numerical Grid Generation," in *The Finite Analytical Method in Flows and Heat Transfer*, New York, Taylors and Francis, 2000, ch. 14, Sec. III, pp. 155-160.
13. Chang C. S., and Huang C. C., "Pressure drop across a Perforated-Plate Distributor in a Gas Fluidized Bed," *Journal of Chemical Engineering of Japan*, Vol. 33, No. 2, pp 722-728
14. Chris Higman and Maarten van Burgt "Introduction" in *Gasification*, 2nd ed., Oxford, UK: Elsevier pp. 1-7, 2003, ch.1, sec.1, pp. 1-7.
15. D. A. Nemtsov and A. Zabaniotou, "Mathematical modelling and simulation approaches of agricultural residue air gasification in a bubbling fluidized bed reactor," *Chemical Engineering Journal*, Vol. 143, pp. 10-31, 2008.
16. Daizo Kunii, Octave Levenspiel, "Fluidization Engineering," 2nd Edition
17. D. Geldard, "Types of Gas Fluidization," *Powder Technology*, Vol. 7, 1973.

18. D.Sathiyamoorthy, Masayuki Horio, "On the influence of aspect ratio and distributor in gas fluidized bed," *Chemical Engineering Journal*, Vol. 93, Issue 2, pp. 151-161 June 2003.
19. Engstrom F, Pai D. Fluidised bed combustion technology—the past, the present, the future. *Modern Power Systems*, pp. 21–26, 1999.
20. Fre'de'ric Depypere, Jan G. Pieters, Koen Dewettinck, "CFD analysis of air distribution in fluidised bed equipment," *Powder Technology* Vol.145, pp. 176–189, 2004.
21. F.Hernandez-Jimenez, S. Sanchez-Delgado, A. Gomez-Garcia, A. Acosta-Iborra. " Comparison between two fluid model simulations and Particle Image Analysis & Velocimetry (PIV) results for a two-dimensional gas-solid fluidized bed," *Chemical Engineering Science*, Vol. 60, pp. 3753-3772, 2011.
22. Falah Alobaid, Jochen Ströhle, Bernd Epple, "Extended CFD/DEM model for the simulation of circulating fluidized bed," *Advanced Powder Technology*, Vol. 24, Issue 1, pp. 403-415, January 2013.
23. G. A. Bokkers, M. van Sint Annaland and J. A. M. Kuipers, "Mixing and segregation in a bidisperse gas-solid fluidised bed: a numerical and experimental study," *Powder Technology*, Vol. 140, pp. 176-186, 2004.
24. Gaurav Agarwal, , Brian Lattimer, Srinath Ekkad, Uri Vandsburger, "Influence of multiple gas inlet jets on fluidized bed hydrodynamics using Particle Image Velocimetry and Digital Image Analysis," *Powder Technology*, Vol. 214, Issue 1, pp 122–134, 25 November 2011.
25. J.C. Schouten, M.L.M. Vander Stappen, C.M. Van Den Bleek, "Scale-up of chaotic fluidized bed hydrodynamics," *Chemical Engineering Science*, Vol. 51, Issue 10, Pages 1991–2000, May 1996.

26. J. M. Paiva, C. Pinho, R. Figueiredo, "The Influence of the Distributor Plate on the Bottom Zone of a Fluidized Bed Approaching the Transition from Bubbling to Turbulent Fluidization," *Chemical Engineering Research & Design*, Vol. 82, Issue 1, pp. 25–33, January 2004.
27. Jingyuan Sun, Yefeng Zhou, Congjing Ren, Jingdai Wang n, Yongrong Yang, "CFD simulation and experiments of dynamic parameters in gas–solid fluidized bed," *Chemical Engineering Science*, Vol. 66, pp. 4972–4982, 2011.
28. Joshua Drake, Hydrodynamic Characterization of 3D Fluidized Beds Using Noninvasive Techniques," Graduate Theses and Dissertation Paper PhD, Iowa University, 2011
29. Juliána, F. Galluccib, M. van Sint Annalandb, J. Herguido, M. Menéndez, "Coupled PIV/DIA for fluid dynamics studies on a Two-Section Two-Zone Fluidized Bed Reactor," *Chemical Engineering Journal*, Vol. 207–208, pp. 122–132, 1st October 2012.
30. Justin A. Gantt and Edward P. Gatzke, (2006, August), Kinetic Theory of Granular Flow Limitations for Modeling High-Shear Mixing, "Ind. Eng. Chem. Res.," Vol. 45 (20), pp. 6721–6727
31. K. Johansson, B.G.M. van Wachem, A.E. Almstedt, "Experimental validation of CFD models for fluidized beds: Influence of particle stress models, gas phase compressibility and air inflow models," *Chemical Engineering Science*, Vol. 61, pp. 1705 – 1717, 2006.
32. K. D. Kafuia, C. Thornton, M. J. Adams, "Discrete particle-continuum fluid modelling of gas–solid fluidised beds" *Chemical Engineering Science*, Vol. 57, pp. 2395 – 2410, 2002.
33. Liang Yu, Jing Lu, Xiangping Zhang, Suojiang Zhang, "Numerical simulation of the bubbling fluidized bed coal gasification by the kinetic theory of granular flow (KTGF)," *Fuel*, Vol. 86, pp. 722–734, 2007.

34. Lu Huilin,, He Yuronga, Dimitri Gidaspow, “Hydrodynamic modelling of binary mixture in a gas bubbling fluidized bed using the kinetic theory of granular flow,” *Chemical Engineering Science*, Vol. 58, Issue 7, pp. 1197–1205, April 2003.
35. Lu Huilin,, Zhao Yunhuaa, Jianmin, Dimitri Gidaspowc, Li Weia, “Investigation of mixing/segregation of mixture particles in gas–solid fluidized beds,” *Chemical Engineering Science*, Vol. 62, Issues 1–2, pp. 301–317, January 2007.
36. Lun C. K. K., Savage S. B., Jerrey D. J. and Chepurniy N., "Kinetic Theories for Granular Flow: Inelastic Particles in Couette Flow and Slightly Inelastic Particles in a General Flow Field," *Journal of Fluid Mechanics*, Vol. 140, pp 223-256, 1984.
37. Li Chen, Yuguo Li, Richard Manasseh, “The coalesce of bubbles, a numerical study,” Third International conference of Multiphase, ICMF, 1998
38. M.T. Dhotre, J. B. Joshi, “ Design of a gas distributor: Three Dimensional CFD Simulation of a Coupled System,” *Chemical Engineering Journal*, Vol. 125, pp. 149-163, 2007
39. Mahdi Hamzehei, (2011, March 7) “CFD Modeling and Simulation of Hydrodynamics in a Fluidized Bed Dryer with Experimental Validation,” *International Scholar Research Network ISRN Mechanical Engineering*, [Online] Vol. 2011, Article 1D 131087. downloads.hindawi.com/isrn/me/2011/131087.pdf
40. Maryam Karimi, Navid Mostoufi, Reza Zarghami, , Rahmat Sotudeh-Gharebagh, “A new method for validation of a CFD–DEM model of gas–solid fluidized bed,” *International Journal of Multiphase Flow*, Vol. 47, pp. 133–140, December 2012.
41. Mengxi Liu, , Yongmin Zhang, Hsiaotao Bi, , John R. Grace, ,Yadong Zhu, “Non-intrusive determination of bubble size in a gas–solid fluidized bed: An evaluation, *Chemical Engineering Science*,” Vol. 65, Issue 11, pp. 3485–3493, 1 June 2010.

42. N. H. Florin and A. T. Harris, "Enhanced hydrogen production from biomass with in situ carbon dioxide capture using calcium oxide sorbents," *Chemical Engineering Science*, vol. 63, pp. 287-316, 2008.
43. Prabir Basu, (2006) "*Combustion and Gasification in Fluidized bed*," Taylor and Francis.
44. Paulose, M M "Hydrodynamic Study of Swirling Fluidized Bed and the Role of Distributor," PhD Thesis, School of Engineering, Co Chin Uni. Of Science and Tech, Kochi India, 2006.
45. Saxena C. S., Chatterjee A., and Patel R. C.' "Effect of Distributors on Gas-Solid Fluidization," *Powder Technology*, Vol. 22, pp. 191-198, March–April 1979.
46. Seyyed Hossein Hosseini, Goodarz Ahmadi, Rahbar Rahimi, Mortaza Zivdar, Mohsen Nasr Esfahany, "CFD studies of solids hold-up distribution and circulation patterns in gas–solid fluidized beds," *Powder Technology*, Vol. 200, Issue 3, pp. 202-215, 28 June 2010,.
47. S. S. Sadaka, A. E. Ghaly and M. A. Sabbah, "Two phase biomass air-steam gasification model for fluidized bed reactors: Part I-model development," *Biomass and Bioenergy*, Vol. 22, pp. 439-462, 2002.
48. Shankar Subramaniam, "Lagrangian-Eulerian methods for multiphase flows," *Progress in Energy and Combustion Science*, Vol. 39, Issue 2-3, Pg. 215-245, 2013.
49. Sh. Saberi, B. Saberi, K. Shakourzadeh, P. Guigon, "Comparative study of tuyere designs of fluidized beds," *The Chemical Engineering Journal and the Biochemical Engineering Journal*, Vol. 60, Issue 1-3, Pg. 75-79, 1995

50. Sobrino, Celia; Ellis, Noko; Vega, Mercedes de, "Distributor effects near the bottom region of turbulent fluidized beds," *Powder Technology*, Vol. 189(1), pp. 25-33, Jan. 2009.
51. Swarbrick J, Boylan J.C (1992), "*Fluid bed dryer, granulator and coaters*," Encyclopaedia of pharmaceutical technology," Marcel Dekker INC, New York, Volume- 6, pp. 171-173
52. Toomey, R.D., and H.F. Johnson, *Chemical Engineering Progr. Symposium Ser. No. 5*, 49, 51, 1953.
53. V. Tanneura,, C. Jousot-Dubienb, B. Fournela, S. Sarradeb, B. Freisse, F. Marciacqc, G.M. Riosd, "Group A particle fluidization in supercritical carbon dioxide: Effect of operating conditions on fluidization efficiency," *Powder Technology* vol. 187 part 2 pp. 190-194
54. Volker Wiesendorf, Joachim Werther, "Capacitance probes for solids volume concentration and velocity measurements in industrial fluidized bed reactors," *Powder Technology* Volume 110, Issues 1–2, pp. 143–157, 1 May 2000.
55. Winkler, F, "Verfahren zum Herstellen von Wasserglas," German Patent 437,970, 1992.
56. Wei-Ming Lu, Sheau-Pyng Ju, Kuo-Lun Tung, Yu-Chang Lu, "Stability analysis of perforated plate type single stage suspension fluidized bed without down comer," *Korean Journal of Chemical Engineering*, Vol. 16, Issue 6, pp. 810-817, November 1999.
57. Yates, J. G. and S. J. R. Simons, "Experimental methods in fluidization research." *International Journal of Multiphase Flow*, Vol. 20, pp. 297-330, 1, August 1994.

